Naval Research Laboratory
Washington, DC 20375-5320

NRL/MR/6790--93-7403

Pinched Propagation of High-Power, Pulsed Electron Beams for Welding and Materials Processing Applications

RICHARD F. FERNSLER
RICHARD F. HUBBARD
MARTIN LAMPE

Beam Physics Branch
Plasma Physics Division

January 3, 1994

Approved for public release; distribution unlimited.

REPORT DOCUMENTATION PAGE

Form Approved
OMB No. 0704-0188

1. AGENCY USE ONLY (*Leave Blank*)	2. REPORT DATE	3. REPORT TYPE AND DATES COVERED
	January 3, 1993	Interim

4. TITLE AND SUBTITLE

Pinched Propagation of High-Power, Pulsed Electron Beams for Welding and Materials Processing Applications

5. FUNDING NUMBERS

ARPA Order #7781

6. AUTHOR(S)

Richard F. Fernsler, Richard F. Hubbard, and Martin Lampe

7. PERFORMING ORGANIZATION NAME(S) AND ADDRESS(ES)

Naval Research Laboratory
Washington, DC 20375-5320

8. PERFORMING ORGANIZATION REPORT NUMBER

NRL/MR/6790--93-7403

9. SPONSORING/MONITORING AGENCY NAME(S) AND ADDRESS(ES)

Office of Naval Research
800 North Quincy Street
Arlington, VA 22217-5660

ARPA, Arlington, VA 22203
NSWC, Silver Spring, MD 20903-5000

10. SPONSORING/MONITORING AGENCY REPORT NUMBER

11. SUPPLEMENTARY NOTES

12a. DISTRIBUTION/AVAILABILITY STATEMENT

Approved for public release; distribution unlimited.

12b. DISTRIBUTION CODE

13. ABSTRACT (*Maximum 200 words*)

Electron beams are used commercially as intense heating sources for welding and related materials processing applications. The beams used for welding operate continuously with energy up to 200 keV and current ~ 1 A. Because these beams are severely degraded by propagation in air over any substantial range, most present-day electron-beam welders require vacuum pumping and precision focusing, which has severely restricted utilization of the technology. Over the past few decades, a different class of electron-beam generators has been developed that produces pulsed beams with energies of several MeV, currents of 1 kA or more, radii as small as 1 mm, pulse lengths of tens of ns, and pulse repetition rates up to several kHz. We show here that beams of this type can propagate in ambient air, in a tightly pinched mode and with acceptable stability, over distances of a few tens of cm. We determine the constraints on the choice of beam parameters, due mainly to the effects of gas scattering and the resistive hose instability. We show that stability can be enhanced, and the acceptable parameter range extended considerably, by using a narrow conducting pipe filled with air or another gas to guide the beam to the workpiece.

14. SUBJECT TERMS

Relativistic electron beam
Welding
Resistive hose instability
Nordsieck
Material processing

15. NUMBER OF PAGES

59

16. PRICE CODE

17. SECURITY CLASSIFICATION OF REPORT	18. SECURITY CLASSIFICATION OF THIS PAGE	19. SECURITY CLASSIFICATION OF ABSTRACT	20. LIMITATION OF ABSTRACT
UNCLASSIFIED	UNCLASSIFIED	UNCLASSIFIED	UL

NSN 7540-01-280-5500

Standard Form 298 (Rev. 2-89)
Prescribed by ANSI Std 239-18
298-102

CONTENTS

I. INTRODUCTION 1

II. REVIEW OF ELECTRON BEAM PROPAGATION PHYSICS 5
- A. Beam Production and Conditioning 5
- B. Self-Pinched Propagation 6
- C. Elastic Gas Scattering 8
- D. Beam Energy Loss and Erosion 11
- E. Effective Pinch Current 12

III. RESISTIVE HOSE INSTABILITY 15
- A. General Properties 15
- B. Phase-Mixing of Electron Trajectories 16
- C. Nordsieck Expansion 20
- D. Wall Stabilization by a Metallic Pipe 20
- E. Estimating the Hose Gain 23

IV. PROPAGATION EXAMPLES 24
- A. HEEB Parameter Choice 24
- B. Particle-Simulation Results 25

V. OTHER ISSUES 27
- A. Gas Heating 27
- B. Beam Deflection 28
- C. Matching 29

VI. CONCLUSION 31

ACKNOWLEDGMENTS 33

REFERENCES 34

APPENDIX 37

PINCHED PROPAGATION OF HIGH-POWER, PULSED ELECTRON BEAMS FOR WELDING AND MATERIALS PROCESSING APPLICATIONS

I. INTRODUCTION

Many industrial processes require that a localized heat source be applied to a metal, ceramic, or other material. These processes include welding, bonding, cutting, annealing, surface hardening, and fabrication of advanced materials. Although conventional heat sources are commonly employed for these purposes, lasers and electron beams have also been used. Electron beams are especially promising because they offer high irradiance, the ability to pass through metal vapors with little degradation, and high "wallplug-to-workpiece" efficiency.[1] For example, compared with traditional arc welders, electron beams[1-9] can produce narrower welds at much higher speeds and lower heat input.[1-3]

Nevertheless, electron beam processing is not widely used commercially, except in the automotive industry in the United States where atmospheric electron beam welding has been used since the mid-sixties.[3] In part, this is due to the limitations of the technology that has been employed to date. For example, present-day commercial electron beam welders typically operate at energies less than 200 keV and at average currents less than 1 amp. When operating in the atmosphere at these energies, scattering of the electrons off air molecules causes rapid expansion of the beam. To reduce beam divergence, magnetic focusing[1,3,4] is deployed at the point where the beam is released into the atmosphere. Beam expansion can be further reduced by taking advantage of the reduction of air density within the beam-heated air channel ("hole-boring"),[5,9] or by propagating the beam within a helium jet rather than open air.[2,5] Nevertheless, the depth of focus remains limited, and the beam source must be operated within a few cm of the workpiece. A larger standoff would be far more attractive because it would ease target setup, produce deep and parallel weld joints, and minimize variations in beam focus that result from power-supply ripple, fluctuations in the weld-cavity depth, or curvature of the workpiece surface.[4,6] Perhaps most significantly, splash-back of debris into the accelerator would be reduced; at present, splash-back is a major problem[6] due to arcing within the accelerator. To minimize arcing[4] (and also to minimize the need for x-ray shielding[5]), beam energies greater than 200 keV have generally been avoided.

Many of these limitations can be circumvented by operating in vacuum, but this profoundly changes the processing conditions and is unacceptable for certain applications. At

Manuscript approved November 17, 1993.

best, the use of a vacuum system increases the cost considerably, both in terms of equipment needed and operating time lost to chamber evacuation.[6]

Another consideration is that at these energies, the electrons penetrate only a short distance into the workpiece (10-100 microns into steel, for example), so that the beam deposition is confined to the surface. As is the case with laser welding and conventional heat sources, the interior is heated through a combination of thermal conduction and convection. However, these processes reduce system efficiency by spreading the energy to areas outside the target zone, and they produce a "nail-head" profile in which the weld radius decreases with depth.[7] Furthermore, the weld joint is vulnerable to irregularities in the target material and the cleanliness of its surface.[6,8] An additional problem specific to electron beams is joint detracking, caused by magnetic beam deflection due to magnetic materials, asymmetrical currents in the liquid weld pool, or thermoelectric currents produced by the heating of dissimilar metals.[4,6,8]

As has been recently pointed out,[10] many of these problems can be eliminated by using high current, pulsed electron beams with energy in the relativistic range (> 1 MeV). For the sake of brevity, we shall adopt the terminology of a recent workshop[11] on electron-beam processing, and refer to beams of this type as high-energy electron beams (HEEB). Pulsed rather than dc operation allows much higher accelerating voltages to be applied without insulator breakdown,[12] and research laboratories routinely utilize this technology to produce electron beams with energies of several MeV, currents of 1 kA or more, and pulse lengths of 10-1000 ns. The beams have been generated using diodes, betatrons, and staged induction accelerators.[13-18] Reliable and reproducible operation has been achieved for many millions of shots and at pulse repetition rates up to 1 kHz.[16] Although x-ray production is much higher at these energies, adequate shielding has not been a problem. In fact, the production of copious x-rays offers the potential for real-time, in-situ diagnostics. However, for typical materials processing applications, the beam energy should be restricted to less than 10 MeV, in order to avoid nuclear activation of long-lived radioactive isotopes in the target. It should be noted that low-current, non-pulsed electron beams in this energy range are already in use for certain industrial materials processes.[19-21]

Pulsed beams with high current and high electron energy offer significant advantages over the dc low-power beams used presently. The first class of advantages relates to propagation to the workpiece. High electron energy, in itself, makes the beam "stiff" and thus less sensitive to

stray magnetic fields or gas scattering.[22] This reduces joint mistracking and permits a somewhat increased standoff distance. More importantly, beams with both high energy and high current (in the kA range) can propagate in dense gas in a self-pinched mode, because the beam space charge is neutralized by beam-ionized plasma. As we shall show, self-pinching permits stable, tight propagation through tens of cm or more of ambient air. Adequate standoff can then be provided, without need of vacuum pumping. A second class of advantages relates to the very different way in which a HEEB interacts with the workpiece. High-energy beams deposit energy nearly instantaneously and deep into the target material. For example, the range of 1-10 MeV electrons in dense materials like steel or titanium is approximately 0.1-1 cm. This deep penetration makes material processing much less dependent on the condition and cleanliness of the surface. Furthermore, because the energy is deposited in a time much shorter than the hydrodynamic or thermal conduction times on which the material responds, the heating is more efficient and the spatial extent of the heat-affected zone[8] is reduced, which can be important for applications like welding. For applications like hardening, it may be useful to use pulse energy densities that are large enough to drive localized shocks as well as heat the material. For other applications, it may be convenient to vary the beam parameters during the pulse train, to tune the time dependence of the energy deposition (as needed, for example, when making continuous weld joints[4]). In short, high-energy, high-current, pulsed electron beams offer new capabilities and the potential to overcome many of the limitations of the commercial devices in use today.

A large number of applications for HEEB welding and materials processing has been suggested,[11] but the beam parameters required for these applications are diverse and not well known at the present time. Some applications, such as welding, require small beam radii ($a_b \sim 0.1$ cm) and high source brightness from the accelerator. Other applications, such as bonding, surface modification, and materials fabrication, typically require beams with larger radii and lower brightness, but possibly with larger total current. This paper addresses the limits imposed on the choice of HEEB parameters by the physics of beam propagation in the atmosphere or other dense gas, over distances of a few tens of cm from the accelerator to the target. For specificity, we further restrict the analysis to a "welding" regime where $a_b \sim 0.1$ cm, and a "materials processing" regime where we arbitrarily assume that $a_b \sim 1$ cm. Everything else being equal, it is always easier to propagate a beam with a larger radius.

The propagation of high-power electron beams is a complic ·d field that has been the subject of an extensive literature. To analyze the various physics issues, we draw on much of this previous work. However, we shall point out that there are significant physical differences between the parameter regime of interest here (e.g., for welding, beam currents $I_b \sim 1$ kA, beam radius $a_b \sim 0.1$ cm, propagation distance $z_t \sim 30$ cm) and the focus of most of the earlier work ($I_b > 10$ kA, larger a_b, and very long z_t). In Sec. II, we review HEEB generation and the physics of self-pinching in dense gas. In Sec. III we discuss the resistive hose instability and its impact on beam propagation and energy deposition at the target; several stabilizing effects, including phase-mixing, gas scattering, and pipe guiding, are shown to be important. In Sec. IV, we illustrate the propagation limitations on HEEB using both analytic examples and numerical simulations computed using a three-dimensional, fully electromagnetic particle code (SARLAC) developed for studying the propagation of relativistic electron beams in the atmosphere. Miscellaneous issues such as gas heating, deflection from stray fields, and accelerator interface problems are discussed in Sec. V. The detailed mathematical treatment of hose instability is considered in the Appendix.

II. REVIEW OF ELECTRON BEAM PROPAGATION PHYSICS

A. Beam Production and Conditioning

The production of high-power electron beams utilizes pulsed power technology that has been under development since the 1960's. In the most common configuration, a prime power supply is connected to a Marx generator consisting of a series of capacitors that are charged in parallel and discharged in series. The output from the Marx generator is usually passed to an intermediate storage capacitor, followed by a pulse forming line (PFL). The high voltage, short-pulse output from the PFL is then switched into a load. If the load is a diode, electrons are produced at the cathode and accelerated towards a positive anode. High-power diodes are generally single-stage devices inherently limited to a few megavolts or less, and in the past they have usually been single-pulse research machines incapable of the high throughput needed for commercial applications. However, there has been recent interest in developing high average power, pulsed diodes for applications like high-power microwaves.[23]

Higher voltages can be generated by deploying a series of linear induction accelerating cavities. This is the basis of several large high-current accelerators, including the RADLAC accelerator at Sandia National Laboratories[15] and the Experimental Test Accelerators (ETA and ETA-II) and the Advanced Test Accelerator (ATA) at Lawrence Livermore National Laboratory.[16-18] ETA-II is particularly of interest because its brightness, pulse repetition rate, current, and energy are in an appropriate regime for welding and materials processing. However, all of these devices are large and expensive, and their limited number of pulses in a burst makes the *average* power insufficient for most commercial applications.

New accelerator concepts are currently being developed that may soon be capable of delivering high average power at a cost low enough to be of commercial interest. The SNOMAD device,[12] which is being developed at Science Research Laboratory, uses solid-state switches to produce 0.5 kA, 0.5 MeV beams with a pulse repetition frequency (PRF) up to 5 kHz. Additional modules will raise the energy to 1.5 or 2.5 MeV in the near future. The Repetitive High Energy Pulsed Power (RHEPP) system[12] being developed at Sandia National Laboratories, uses a magnetic pulse compressor to drive a linear induction voltage adder with a diode load. This system is designed to accelerate either electron or ion beams, with higher currents (~25 kA)

but lower PRF (~120 Hz) than SNOMAD. The pulsed power system operates at 0.9 MV, with plans to produce a 2.5 MeV beam.

Previous studies of *long-range* beam propagation have focused on the development and use of post-accelerator conditioning cells[24-26] to suppress the resistive hose instability. We shall discuss this beam-plasma instability in Sec. III, and shall show that it is a matter of some concern for the present applications. However, we shall conclude that the use of beam conditioning is not necessary or even useful for the relatively short-range propagation considered here.

B. Self-Pinched Propagation

In using HEEB for welding and materials processing, we wish to deliver a beam of high current density onto a target piece located several tens of cm from the accelerator in ambient air or other dense gas. On its way to the target, the beam collides with gas molecules, expands as a result of its transverse pressure, and may suffer electromagnetic instabilities. At some point, these processes degrade the beam to the extent that it is no longer useful. In this and the following sections, we review the physics of beam propagation in dense gas and determine the constraints that propagation imposes on HEEB applications.

We simplify the analysis by assuming the beam to be highly relativistic and paraxial, meaning that the beam electrons travel in the z direction with an axial velocity $v_z \approx c$ and a transverse velocity $v_\perp << v_z$. These assumptions decouple the transverse motion of the beam from its longitudinal motion, and permit us to describe beam expansion and contraction in terms of a transverse beam temperature, $T_\perp = <\gamma m v_\perp^2/2>$, where m is the electron rest mass and $\gamma = (1-v^2/c^2)^{-1/2} >> 1$ is the relativistic mass factor. In what follows, we shall assume that γ is the same (mono-energetic) for all electrons in a given beam slice. These assumptions are appropriate for HEEB, but not for the low-energy beams conventionally used for welding and materials processing.

All beams are produced with a finite temperature $T_\perp$, and this temperature increases as the beam collides with gas molecules on its way to the target. In the absence of a radial pinch force, the dispersion of velocity angles associated with $T_\perp$ causes the beam to expand until it is ultimately too tenuous for the desired application. The useful range can be extended, however, by providing a pinch force. For example, a solenoidal magnetic field can be applied to confine

the beam, although this is often impractical because of geometrical constraints or the cost of the field coils.

If the beam is sufficiently intense and propagating in dense gas, a self-pinch force develops naturally as the beam ionizes the gas and creates a conducting plasma. The plasma fully neutralizes the beam space charge but is too resistive to fully neutralize the beam current. As a result, a finite net current (equal to the sum of the beam current and the plasma return current) is left flowing parallel to the beam. The net current pinches the beam magnetically and retards its expansion. The plasma thus enables the beam to propagate in self-pinched equilibrium without external guide fields. Self-pinched propagation is the feature that makes HEEB welding and materials processing possible with significant standoff in the atmosphere. Figure 1 provides a conceptual illustration of self-pinched propagation of an intense beam to a target.

In self-pinched equilibrium, the magnetic pinch force from the net current balances the transverse beam pressure:

$$\frac{\partial}{\partial r}\,(n_b T_\perp) = -en_b\beta B_\theta = -en_b\beta\,\frac{2i_n(r)}{rc}\ . \qquad (1)$$

Here n_b is the beam density, e is the electron charge, $\beta \approx 1$ is the axial beam velocity normalized to the speed of light c, B_θ is the azimuthal magnetic field, and $i_n(r)$ is the net current enclosed within radius r. Integrating Eq. (1) twice yields the Bennett pinch condition for the average beam temperature:[27]

$$T_\perp = T_B \equiv \frac{e\beta I_{eff}}{2c}\ , \qquad (2)$$

where

$$I_{eff} = \frac{2}{I_b}\int_0^\infty dr\,\frac{\partial i_b}{\partial r}\,i_n(r)\ . \qquad (3)$$

Here I_b is the total beam current, $i_b(r)$ is the beam current within radius r, and I_{eff} is termed the effective pinch current. If there is no plasma return current, $i_n(r) = i_b(r)$ and $I_{eff} = I_b$.

Lee[27] has shown that gas scattering causes a self-pinched beam to evolve to an isothermal state, $T_\perp = T_B$ for all r, in which the beam density assumes a Bennett profile:

$$n_b(r) = \frac{I_b}{e\beta c\pi a_b^2} \frac{1}{(1+r^2/a_b^2)^2} , \qquad (4)$$

where a_b is the half-current radius. In this equilibrium state, the individual beam electrons are not localized at fixed r but undergo sinusoidal-like betatron trajectories about the beam axis, with a characteristic axial wavelength given by

$$\lambda_\beta = 2\pi a_b (I_A/I_{eff})^{1/2} , \qquad (5)$$

where $I_A = \beta\gamma mc^3/e = 17\beta\gamma$ kA is the Alfven current. The distance λ_β is termed the average betatron wavelength, and it characterizes the propagation distance needed for equilibration. For paraxial beams, $\lambda_\beta >> a_b$.

C. Elastic Gas Scattering

Elastic scattering of beam electrons off gas molecules eventually leads to beam expansion, even if the beam is self-pinched (but much more rapidly if the beam is unpinched). Scattering acts as a source of beam transverse energy, given by[22]

$$\left[\frac{dT_\perp}{dz}\right]_s = \frac{4\pi e^4 n_a Z_a (Z_a+1)}{\beta^2\gamma mc^2} \ln\left[\frac{192\beta\gamma}{Z_a^{1/3}}\right] , \qquad (6)$$

where n_a is the atomic number density, Z_a is the atomic number of the gas, and z is propagation distance from the beam source. If the beam is unpinched, its radius increases with z as[28]

$$a_b^2 = a_o^2 - 2a_o\theta_f z + (\theta_f^2+\theta_t^2)z^2 + \frac{2}{3\gamma\beta^2 mc^2}\left[\frac{dT_\perp}{dz}\right]_s z^3 , \qquad (7a)$$

where a_o is the initial beam radius, θ_f is the focusing angle, $\theta_t \equiv (2T_o/\beta^2\gamma mc^2)^{1/2}$ is the initial transverse thermal spread, and T_o is the temperature at the injection point (z = 0) into the gas.

For unpinched beams, the radius can be minimized at target location z_t by using a focusing angle $\theta_f = a_o/z_t$, as can be shown by setting the derivative of Eq. (7a) with respect to θ_f equal to zero. The radius at z_t is then given by

$$a_b^2(z_t) = \theta_t^2 z_t^2 + \frac{2}{3\gamma\beta^2 mc^2}\left(\frac{dT_\perp}{dz}\right)_s z_t^3 \quad . \tag{7b}$$

Thus a minimum beam spot size $a_b(z_t)$ is set by both the initial thermal spread and the additional velocity spread resulting from gas scattering. For $z_t = 30$ cm in atmospheric air, gas scattering alone restricts the radius to $a_b(z_t) > 1$ cm for $\gamma \leq 21$ (10 MeV).

In Fig. 2 we plot $a_b(z)$ for an unpinched beam propagating in full density air with $a_o = 0.1$ cm, optimum focusing angle $\theta_f = 0.003$, initial thermal spread $\theta_t = 0.002$, and energy $\epsilon_o = 3$, 5 and 10 MeV. As is evident, the beam remains narrow for only a few cm of propagation, expanding to $a_b > 1$ cm at $z \geq 30$ cm. While such radii might be acceptable for materials processing, they are far in excess of the typical requirement for welding, $a_b(z_t) \approx 0.1$ cm. The bottom (dashed) curve in Fig. 2 shows the propagation of the same 10 MeV beam in vacuum ($n_a = 0$). In this case, the beam focuses to $a_b(z_t) = \theta_t z_t = 0.06$ cm at $z_t = 30$ cm. Equations (6) and (7) indicate that beam expansion in air can be decreased by directing a jet of gas of low atomic number (e.g., helium) in the path of the beam,[2,5] or by allowing the beam to heat the air and thus "bore" a reduced-density channel in it.[9] Both techniques have been shown to improve the performance of conventional electron beam welders operating in full density air, but the performance is still inferior to that achieved in vacuum.[3,6]

The presence of a pinch force reduces the expansion rate and changes the nature of the expansion process. If the beam power is sufficient, the beam maintains a self-pinched equilibrium satisfying Eq. (2). As scattering adds to the beam's transverse thermal energy, the beam expands adiabatically to maintain the pressure balance condition, $T_\perp = T_B$. The beam density then decreases exponentially according to

$$\frac{1}{n_b}\frac{\partial n_b}{\partial z} = -\frac{1}{T_B}\left(\frac{dT_\perp}{dz}\right)_s \quad . \tag{8}$$

The beam radius, which scales as $n_b^{-1/2}$ by particle conservation, therefore undergoes "Nordsieck expansion,"[27]

$$a_b(z) = a_o \exp(z/L_N) , \tag{9}$$

where the Nordsieck length $L_N = 2T_B/(dT_\perp/dz)_s$ is proportional to γI_{eff} to lowest order. A more careful analysis by Hughes and Godfrey[29] has shown that large-angle scattering weakens the dependence of L_N on γI_{eff}, and yields an approximate expression in the HEEB parameter regime,

$$L_N \simeq 380 \frac{(\gamma I_{eff})^{0.9}}{Z_a(Z_a+1)\rho} \text{ cm} , \tag{10}$$

where I_{eff} is in kA and $\rho = n_a/5.4\text{x}10^{19}$ cm^{-3} is the atomic number density in atmospheres (atm) of STP air. In air, $Z_a = 7.2$ so that $L_N \simeq 6.4\rho^{-1}(\gamma I_{eff})^{0.9}$ cm.

Equations (9) and (10) show that γI_{eff} must be large to limit beam expansion due to gas scattering. It is convenient to define an expansion factor

$$g_a \equiv a_{max}/a_o , \tag{11}$$

where a_{max} is the maximum beam radius allowed at the target. The Nordsieck length must then satisfy $L_N > z_t/\ln(g_a)$, so that γI_{eff} must exceed a minimum value,

$$\gamma I_{eff} > \left[\frac{z_t}{380 \text{ cm}} \frac{Z_a(Z_a+1)\rho}{\ln(g_a)}\right]^{1.1} \text{kA} . \tag{12}$$

As an illustration, consider a beam that propagates a distance $z_t = 30$ cm in atmospheric air ($\rho = 1$). If we require $g_a = \sqrt{2}$, then it is necessary that $L_N \gtrsim 3z_t = 90$ cm, and therefore that $\gamma I_{eff} \gtrsim 20$ kA. I_{eff} cannot exceed I_b for self-pinched beams, and we shall see in Sec. II-E that $I_{eff} \simeq I_b$ for the cases of interest. Thus the pulsed beam power P must satisfy $\gamma I_b \gtrsim 20$ kA, or roughly P > 10 GW. If radiation safety limits the beam energy to 10 MeV ($\gamma \leq 21$), the beam current I_b must exceed 1 kA.

Figure 3 shows plots of $a_b(z)$ from Eqs. (9) and (10), for a beam injected with $a_o = 0.1$ cm, $\theta_f = 0$, $T_\perp$ matched to a pinch current of $I_{eff} = 1$ kA, and at energies of $\epsilon_o = 3$, 5 and 10 MeV in

full density air. The expansion, although often appreciable, is much slower than in the unpinched case plotted in Fig. 2.

We conclude from this discussion that high γ alone (10 MeV) can keep the beam radius to under a few cm over propagation distances of a few tens of cm in atmospheric air or like gases. This may be sufficient for some materials processing applications. However, to keep the beam radius well under 1 cm for applications like welding, self-pinched propagation is needed. For propagation through 30 cm in full atmosphere, a minimum current and power of 1 kA and 10 MW are typically required. We shall use the latter values as our nominal HEEB parameters.

Equations (9) and (10) for self-pinched propagation govern only if the characteristic length λ_β for the beam to establish pressure balance ($T_\perp = T_B$) is shorter than the characteristic expansion length L_N,

$$\lambda_\beta < L_N \ . \tag{13a}$$

This condition is equivalent to the statement that self-pinched expansion occurs only if it is slower than free expansion. Using Eqs. (5) and (10), we can rewrite (13a) as a condition on the beam radius,

$$a_b < \frac{L_N}{2\pi}\sqrt{\frac{I_{eff}}{I_A}} \approx \frac{15}{Z_a(Z_a+1)\rho} I_{eff}^{1.4}\,\gamma^{0.4} \text{ cm} \ , \tag{13b}$$

where I_{eff} is again in kA. In atmospheric air, condition (13b) gives $a_b < 1$ cm for $I_{eff} = 1$ kA and $\gamma \leq 21$. Recall, however, that self-pinching may not be needed if radii at the target in excess of 1 cm are adequate for the application.

D. Beam Energy Loss and Erosion

Collisions with the air molecules not only scatter the beam but also extract energy from the beam. For beam energies $\epsilon \leq 10$ MeV, the dominant loss comes from inelastic collisions at a rate[22]

$$\frac{d\epsilon}{dz} = \frac{4\pi e^4 n_a Z_a}{mc^2\beta^2}\left[\ln\left(\frac{2mc^2\beta^2\gamma^2}{W_o}\right) - \beta^2\right] \ , \tag{14a}$$

where W_o is a typical molecular excitation energy. In atmospheric air, if we use the estimate $W_o \approx 10\,eV$,

$$\frac{d\mathcal{E}}{dz} \approx [2 + 0.4\ \ln(\gamma)]\ \text{keV/cm}. \tag{14b}$$

The collisional energy loss over 30 cm of propagation is thus ~ 0.1 MeV, which is negligible for beam energies of several MeV.

The beam also loses energy to the inductive electric field that arises in response to the beam current. Averaged over the beam pulse, this field satisfies

$$E_z \leq LI_b/\tau_p\ , \tag{15}$$

where τ_p is the pulse duration and L ~ 10 nH/cm is the distributed circuit inductance discussed in Sec. II-E. For $\tau_p \geq 10$ ns and $I_b = 1$ kA, the time-averaged field is 1 kV/cm or less. The beam energy lost over 30 cm of propagation is therefore less than 30 keV per electron, which is negligible. In practice, the ohmic losses are confined mainly to the beam head rather than uniformly distributed over the pulse. This causes the head to lose energy, expand, and erode.[30] The estimate given here shows that the amount of beam eroded is insignificant relative to the pulse duration.

E. Effective Pinch Current

In this section we show that the effective pinch current is essentially equal to the full beam current for the nominal parameters used in HEEB. That is, the plasma formed by the beam in air is sufficiently conducting to neutralize the beam space charge, but is too resistive to neutralize the beam current.

A beam with the high current density required for welding and materials processing ionizes and heats the air through which it passes. According to a simple ionization-recombination model, the plasma electron density n_e evolves as

$$\frac{\partial n_e}{\partial t} \approx \frac{j_b\ d\mathcal{E}/dz}{eW_i} - \beta_r n_e^{\,2}\ , \tag{16}$$

where $j_b = I_b/\pi a_b^2$ is the on-axis beam current density, $d\mathcal{E}/dz \approx 3$ keV/cm is the collisional energy loss rate discussed in Sec. II-D, $W_i \approx 34$ eV is the average energy deposited per plasma electron created,[31] and $\beta_r \sim 5\times10^{-8}$ cm^3/s is the dissociative plasma electron-ion recombination coefficient. After a characteristic time

$$\tau_s = a_b \left(\frac{\pi e W_i}{\beta_r I_b \, d\mathcal{E}/dz} \right)^{1/2}, \qquad (17a)$$

n_e on axis approaches a "saturated" steady state value,

$$n_{eo} = a_b^{-1} \left(\frac{I_b \, d\mathcal{E}/dz}{\pi e W_i \beta_r} \right)^{1/2}. \qquad (17b)$$

For the "welding" beam with $I_b = 1$ kA and $a_b = 0.1$ cm, the saturation time in atmospheric air is $\tau_s \approx 1$ ns, which is much shorter than the pulse duration τ_p for a typical case with $\tau_p \geq 10$ ns. The plasma density n_e, and conductivity $\sigma = e^2 n_e/m\nu$, can thus be treated as constant over most of the pulse; here ν is the plasma electron collision frequency, with a value $\sim 2\times10^{12}$ s^{-1} in atmospheric air. The assumption of constant σ is used later to simplify the analysis of hose instability. In broader beams, where saturation occurs at a later time, it may be necessary to retain the time dependence of σ.

The plasma neutralizes the beam space charge in a time $1/4\pi\sigma$ which is negligibly short ($\ll 1$ ns) for the parameters given above. Electrostatic forces can therefore be safely ignored. Current neutralization, however, persists only for a time $\tau_o \equiv L/R$ which characterizes magnetic field diffusion through the plasma. Here $L \approx (1/c^2)\ln(1+a_w^2/a_b^2)$ is the distributed circuit inductance, $R \approx 1/\pi a_b^2 \sigma$ is the distributed plasma resistance, and $a_w > a_b$ is the effective outer edge[32] of the plasma. Since R steadily decreases as beam ionization increases the plasma conductivity, τ_o is an increasing function of the retarded time $\tau \equiv t - z/\beta c$, which is the time measured after the arrival of the beam head at location z. The saturation of σ due to recombination eventually limits R, and this restricts τ_o to

$$\tau_o \leq \frac{e^2 a_b}{mvc^2} \left[\frac{\pi I_b \, d\epsilon/dx}{eW_i \beta_r} \right]^{1/2} \ln(1+a_w^2/a_b^2) \quad . \tag{18}$$

For the welding beam with I_b =1 kA, a_b = 0.1 cm, and $a_w < 50\ a_b$, the decay time τ_o is always less than τ. The plasma return current induced by the beam then decays essentially instantaneously so that

$$I_{eff} \approx I_b \tag{19}$$

for virtually all of the pulse. All but the early beam head thus feels a strong magnetic force that keeps the beam well pinched on its way to the target. For broader beams, τ_o is larger but still smaller than the pulse duration τ_p in the parameter regime of interest. In that case, I_{eff} approaches I_b gradually so that the beam pinch force increases with τ. This gradual increase causes the beam head to flare, so that a_b decreases with τ. Nordsieck expansion accentuates the flaring as z increases, as seen in the simulations presented in Sec. IV.

III. RESISTIVE HOSE INSTABILITY

A. General Properties

Electron beams propagating through dense gas are subject to a number of instabilities, but the only significant one for the HEEB applications being considered here is the resistive hose instability.[33-39] Resistive hose is a macro-instability in which the beam performs growing snakelike oscillations from side to side, in response to magnetic forces from the plasma. The instability develops as plasma eddy currents induced by the beam motion lag behind the beam by a magnetic diffusion time, due to the resistivity of the plasma. This phase lag causes the transverse beam wiggles to grow in amplitude. Other instabilities are known to occur in beams propagating in gas, but are not relevant to the parameters of interest here. For example, the resistive hollowing instability does not occur in the absence of a strong plasma return current,[40] while the two-stream instability is suppressed by collisions between the plasma electrons and the gas molecules.

Hose instability is characterized by the transverse displacement $x_b(z,\tau)$ of the beam centroid from the desired propagation axis. When x_b grows to large amplitude ($x_b \geq a_b$), the instability spreads out the energy density delivered to the target, and can even cause the beam to miss the target. To avoid these effects, the beam parameters should be chosen to keep hose in the linear regime, $x_b < a_b$. In this regime, x_b is proportional to the initial perturbation x_i, and the hose gain, $g_h(z) \equiv x_{max}(z)/x_i$, is independent of the magnitude of x_i; here $x_{max}(z)$ is the maximum of $x_b(z,\tau)$ within the pulse at a given propagation distance z. Thus, it is convenient to state the hose stability requirement as

$$g_h(z_t) \quad < \quad a_b(z_t)/x_i \ . \tag{20}$$

Although the hose gain g_h is independent of the magnitude of x_i in the linear regime, it is strongly dependent[35] on the temporal variation of x_i with τ. To be conservative, we shall allow for excitation of the most rapidly growing hose perturbations and compute the maximum hose gain possible. Because experience shows that it is difficult to launch a beam with initial perturbations less than a few percent of the injected radius a_o, we shall restrict g_h to be less than 30. In practice, the use of the maximum hose gain may be too restrictive, since the most

dangerous hose perturbations usually occur at frequencies far above the resonant frequencies of the accelerator. See Sec. III-E for further discussion.

In the next three subsections, we estimate the maximum hose gain and the limitations it imposes on the choice of HEEB parameters. Particular attention is given to three stabilizing effects: phase-mixing, Nordsieck expansion, and steering by a metallic pipe surrounding the beam. The latter two effects are shown to be especially important for applications requiring narrow beams.

B. Phase-Mixing of Electron Trajectories

Resistive hose develops from magnetic interactions between the beam and plasma currents, each of which is displaced from the axis of symmetry and from each other. The simplest model of the instability, which we shall call the flexible-rod model, is obtained by representing the perturbations as displacements $x_b(z,\tau)$ of the beam centroid, with no internal distortion (and thus no phase mixing), and characterizing the plasma currents by the location of the net current centroid $x_n(z,\tau)$. For small beam displacements, $x_b << a_b$, a linearized equation for x_b can be obtained by averaging the magnetic force over the radial profile of beam current. In the absence of wall forces ($a_w >> a_b$), this yields[35]

$$\frac{\partial^2 x_b}{\partial z^2} = k_s^2 (x_n - x_b) , \tag{21}$$

where k_s is a characteristic hose wavenumber given by

$$k_s^2 = \frac{1}{I_A I_b} \int_0^{a_w} \frac{dr}{r} \frac{\partial i_b}{\partial r} \frac{\partial i_n}{\partial r} . \tag{22}$$

If the beam and plasma have identical Bennett profiles given by Eq. (4), $k_s = 2\pi(2/3)^{1/2}/\lambda_\beta$, where λ_β is defined in Eq. (5).

An equation for the net-current centroid x_n can be obtained from Ampere's law. As derived by Lee[35] (and in the Appendix), this equation is given in the limit of high γ and high σ by

$$\tau_d \frac{\partial x_n}{\partial \tau} = (x_b - x_n) , \tag{23}$$

where τ_d is a magnetic dipole diffusion time given by

$$\tau_d = \pi a_b^2 \sigma_o / 2c^2 . \tag{24}$$

Here σ_o is the on-axis conductivity. Equations (21), (23), and (24) are appropriate when the plasma return current is negligible, the beam and plasma have identical Bennett profiles, and $x_b << a_b$.

Equations (21) and (23) demonstrate that two parameters characterize hose: the betatron wavelength, $\lambda_\beta \propto k_s^{-1}$, which characterizes the response of the beam; and the dipole diffusion time τ_d, which characterizes magnetic relaxation in the plasma. In general, the amount of hose growth depends on the propagation distance z_t scaled to λ_β and the pulse length τ_p scaled to τ_d. For the "welding" beam with $a_b = 0.1$ cm, $I_b = 1$ kA and $\gamma = 21$, we find $\lambda_\beta \approx 12$ cm and $\tau_d \approx 40$ ps. If $z_t = 30$ cm and $\tau_p \geq 10$ ns, then $z_t/\lambda_\beta \approx 2.5$ while $\tau_p/\tau_d \geq 250$. HEEB welding thus operates in a long-pulse, short-range regime where

$$\tau_p/\tau_d >> 1, \tag{25a}$$

$$z_t/\lambda_\beta \leq \text{few}. \tag{25b}$$

Materials processing applications with $a_b \sim 1$ cm also typically operate in this regime.

Most of the previous theoretical work on hose instability has been in the opposite short-pulse, long-range regime[37] where

$$\tau_p/\tau_d \leq \text{few}, \tag{25c}$$

$$z_t/\lambda_\beta >> 1. \tag{25d}$$

Although strategies developed to control hose in the long-range regime are usually ineffective in the long-pulse regime, there is often a complementary strategy that works. The general rule is that variations of the beam parameters in τ are important when (25c) holds, whereas variations in z are important when (25b) holds. For example, in the long-range regime (25d), the pulse duration τ_p must be limited to a few times τ_d, as specified in (25c), in order to allow the instability to convect[35] out the beam tail before reaching intolerably large amplitude. In the long-pulse regime (25a) of interest here, it is the propagation distance z_t that must be limited, to a few times λ_β as specified in (25b). In a similar vein, hose growth can be reduced in the short-pulse regime (25c) by tailoring the beam so that its emittance, and therefore its radius a_b and betatron wavelength λ_β, decrease significantly (> 20%) over times $\tau \sim \tau_d$, as has been shown by several theoretical[24,25,37] and experimental[26] studies. In the long-pulse regime, however, tailoring is impractical because the variations needed would be excessive (as would be the energy-deposition radius on target). Instead, in the short-range regime, it is variations in λ_β with z (rather than τ) from Nordsieck expansion that helps stabilize hose. A last distinction between the two regimes is the effect of I_b. In the short-pulse regime, large I_b is stabilizing because τ_d increases with I_b. But in the short-range regime, large I_b is destabilizing because λ_β decreases with I_b. In this paper, we concentrate on hose growth in the long-pulse, short-range regime.

We first calculate the hose growth rate using Eqs. (21)-(23), which omit phase-mixing of the electron trajectories. Since the beam and plasma equilibria are assumed to be independent of z and τ, we consider solutions of the form $x \sim e^{-ikz-i\omega\tau}$. We take ω to be real and calculate the corresponding complex value of k, because our primary interest is to calculate hose growth in z. Equations (21) and (23) yield the flexible-rod dispersion relation,

$$(k/k_s)^2 = - \frac{i\omega\tau_d}{1-i\omega\tau_d} \quad . \tag{26}$$

Writing k in terms of real and imaginary components, $k = k_r + ik_i$, we find that the maximum value of k_i is given by

$$k_i^{max} = k_s/\sqrt{8} \quad . \tag{27}$$

This defines the peak growth rate in z, in the absence of phase-mixing of the electron trajectories.

Phase-mixing is a particle effect that occurs because the beam pinch force is anharmonic (i.e., nonlinear in r), which makes the betatron wavelength of each beam electron depend on the amplitude of its orbit. The spread of betatron wavelengths for the electrons in a given beam slice destroys the coherence of hose oscillations in that slice, thereby damping those oscillations. Stated differently, phase-mixing gradually converts the ordered energy of hose motion into beam thermal energy and emittance (with the increase in emittance being small when $x_b << a_b$).

To incorporate phase-mixing in an analytically tractable way, we use the spread-mass model developed by Lee.[35] In this model, the beam is artificially represented as a superposition of "flexible-rod" components corresponding to different electron masses, and thus different betatron wavelengths. The distribution of electron masses is chosen to preserve the average oscillation frequency k_s. This model has been shown to give hose growth rates in good agreement (~ 10 percent) with those from more accurate but involved treatments.[38] An abbreviated description of the model is given in the Appendix. Here we simply quote Lee's result [Eq. (143) of Ref. 35]:

$$k_i^{max} = 0.183\, k_{\beta o} = 0.317\, k_s , \qquad (28)$$

where $k_{\beta o}$ is the maximum (on-axis) betatron oscillation frequency. This peak rate is roughly ten percent smaller than prediction (27), a difference comparable to the accuracy of the spread-mass model itself. Thus, phase-mixing reduces, but only slightly, the hose growth rate in z.

Phase-mixing has a weak effect on hose growth in z because it introduces damping at a rate that is small relative to k_s. The damping has a pronounced effect, however, on growth in τ: by spreading the resonance at k_s, it makes the instability convective rather than absolute.[35] This effect is critical in the long-range regime, but not in the long-pulse, short-range regime of interest here.

C. Nordsieck Expansion

The preceding analysis shows that hose growth increases exponentially with the number of betatron wavelengths λ_β propagated. As a result, any process that increases λ_β suppresses hose. One such process is Nordsieck expansion which causes the beam radius a_b, and therefore λ_β (which is proportional to a_b), to increase with propagation distance z.

A simple estimate of the effects of Nordsieck expansion on hose can be easily made in the "welding" regime. In that regime, γ and I_{eff} are nearly constant with both z and τ, and thus the Nordsieck length, $L_N = L_N(\gamma I_{eff})$, can be taken as constant. From Eqs. (5) and (9), the betatron wavelength can be taken as independent of τ but growing in z as

$$\lambda_\beta(z) = \lambda_\beta(0) \exp(z/L_N) \quad . \tag{29}$$

If hose grows nearly exponentially with the number of λ_β propagated, we expect the hose gain $g_h(z_t)$ to be given by

$$\ln[g_h(z_t)] \simeq \alpha_h \int_0^{z_t} \frac{dz}{\lambda_\beta(z)}$$

$$= \frac{\alpha_h L_N}{\lambda_\beta(0)} \left[1 - \exp(-z_t/L_N)\right] , \tag{30}$$

where α_h is a hose growth coefficient of order unity, whose precise form will be discussed in the next two subsections and specified in Eq. (39).

Equation (30) indicates that Nordsieck expansion begins to reduce hose significantly at distances $z_t \geq L_N/5$, and that it limits the hose gain to $g_h \leq \exp[\alpha_h L_N/\lambda_\beta(0)]$. Although a more formal analysis[37] shows that Eq. (30) is strictly valid only when $L_N > z_t$ and $L_N >> \lambda_\beta(0)$, the restriction is usually unimportant since hose growth is modest outside that regime.

D. Wall Stabilization by a Metallic Pipe

A metallic pipe or "straw" enclosing the beam further suppresses hose as return currents induced in the pipe walls magnetically steer the beam. The return current in the walls of the straw can be represented in the linearized regime as an image line current of magnitude $-I_n$

located at a_w^2/x_n from the center of the straw. Here the net current I_n equals the sum of beam and plasma return currents, and $a_w > a_b >> x_n$ is the radius of the straw. In the present application, we have assumed that $I_n \approx I_b$.

The return current in the straw adds another force component to Eq. (21):

$$\frac{\partial^2 x_b}{\partial z^2} = k_s^2 (x_n - x_b) - \frac{r_b^2}{a_w^2} k_s^2 x_n , \tag{31}$$

where r_b is a characteristic beam radius defined by

$$r_b^2 = \frac{2I_n}{I_A} k_s^{-2} . \tag{32}$$

In general, r_b is comparable to but not equal to the half-current radius a_b. If the beam and plasma have identical Bennett profiles of radius a_b, then $r_b = \sqrt{3} a_b$.

A second effect of the straw is to accelerate the diffusion of the dipole magnetic fields. As shown in the Appendix, the magnetic dipole decay time is reduced to

$$\tau_d \approx \left[1-(a_b/a_w)^2 \ln(1+a_w^2/a_b^2)\right](\pi a_b^2 \sigma_o/2c^2) , \tag{33}$$

in place of Eq. (24). However, since τ_d was already much smaller than the pulse duration τ_p, the reduction has no effect on the hose gain g_h.

For simplicity, in the present discussion we ignore phase-mixing (included in the Appendix) and Nordsieck expansion. Again considering solutions of the form $x \sim e^{-ikz-i\omega\tau}$ with real ω and complex k, Eqs. (21) and (31) give a flexible-rod dispersion relation,

$$(k/k_s)^2 = 1 - \frac{1-r_b^2/a_w^2}{1-i\omega\tau_d} , \tag{34}$$

in place of Eq. (26). The peak growth rate is then computed to be

$$k_i^{max} = \frac{k_s}{\sqrt{8}} \frac{1-r_b^2/a_w^2}{\sqrt{1+r_b^2/a_w^2}} , \qquad (35)$$

in place of Eq. (27). Equation (35) indicates that wall forces reduce the hose growth rate for Bennett profiles by a factor

$$\frac{k_i^{max}(a_w)}{k_i^{max}(\infty)} = \frac{1-r_b^2/a_w^2}{\sqrt{1+r_b^2/a_w^2}} = \frac{1-3a_b^2/a_w^2}{\sqrt{1+3a_b^2/a_w^2}} . \qquad (36)$$

This reduction appears to be consistent with that given by Uhm and Lampe[39] for flat-topped beams.

In Fig. 4 the dashed curve shows the normalized peak growth rate $k_i^{max}/k_{\beta o}$ from Eqs. (27) and (36) for a Bennett beam as a function of a_b/a_w, where $k_{\beta o} = \sqrt{3}k_s$. The solid curve shows the corresponding result as calculated in the Appendix, with phase mixing included. The two results are in good qualitative agreement, indicating that the effect of phase mixing is small. In a typical implementation with $a_w = 3a_b$, Fig. 4 indicates that the presence of the straw cuts the peak growth rate by nearly a factor of two. This allows the beam to propagate nearly twice as far in z for a given hose gain g_h, an improvement that far exceeds the stabilizing effect of either phase-mixing or Nordsieck expansion.

In addition to improving stability, the straw could be used for a variety of other purposes, including the following: (i) Scattering can be reduced by flowing helium through the straw, or by differentially pumping to reduce the air pressure by a factor of five to ten. As we shall see, this can substantially reduce the required beam electron energy. Flowing helium through a straw should be simpler and more economical than blowing a helium jet[2] across open air. (ii) The straw can be used to shield the beam from stray magnetic fields[4] as discussed in Sec. V-B. (iii) The straw can be used for precision corrections to beam pointing. A straight straw can accept a misaligned beam and magnetically steer it through a (typically small) angle

$$dx/dz \leq (a_b/a_w)(2I_b/I_A)^{1/2} . \qquad (37)$$

Alternatively, a curved straw can direct the beam around a radius of curvature which satisfies

$$R \geq (a_w^2/a_b)(I_A/2I_b) \quad . \tag{38}$$

Equations (37) and (38) were derived by requiring that the beam remain within one beam radius of the straw axis.

E. Estimating the Hose Gain

The results of the three previous sections on hose may be combined by setting the hose growth coefficient α_h in Eq. (30) to

$$\alpha_h \simeq 1.63 \frac{1-3a_b^2/a_w^2}{\sqrt{1+3a_b^2/a_w^2}} , \tag{39}$$

where $1.63 = 2\pi(0.317)(2/3)^{1/2}$. This value was obtained using the spread-mass result (28) for k_i^{max} in terms of k_s, and using Eq. (36) for the reduction in hose growth produced by a straw of radius a_w, assuming Bennett profiles. Equations (30) and (39) allow us to estimate the hose gain g_h as a function of the propagation distance z_t, the initial betatron wavelength $\lambda_\beta(0)$ given by Eq. (5), and the Nordsieck length L_N given by Eq. (10).

For the canonical welding parameters of $z_t = 30$ cm, $I_b = 1$ kA, $\gamma = 21$, and $a_o = 0.1$ cm, the predicted hose gain is $g_h < 35$ in open air, and it drops to $g_h < 8$ if a straw of radius $a_w = 3a_b = 0.3$ cm is used. In the former case, the transverse beam displacements x_i at the accelerator would have to be less than a few percent of a_o to satisfy criterion (20) at the target; in the latter case, x_i could be as large as 10 percent of a_o, which is well within present accelerator capabilities. Moreover, as mentioned in Sec. III-A, the restrictions on x_i are conservative, because they apply only if the most rapidly growing hose frequencies in τ are excited. For the canonical welding beam, the most dangerous hose frequencies ($\omega\tau_d \sim 1$) occur at a few GHz. If these frequencies are not excited or are excited only at very low levels, the restrictions on x_i could be relaxed.

IV. PROPAGATION EXAMPLES

A. HEEB Parameter Choice

As discussed earlier, the two main propagation issues affecting HEEB operation are beam expansion and the resistive hose instability. Expansion must be limited to prevent the beam from becoming too broad on target, and hose growth must be limited to prevent the beam from wandering off target. We have expressed the former limit in terms of an allowed expansion factor g_a and the latter limit in terms of an allowed hose gain g_h. As Eqs. (5), (12) and (30) indicate, self-pinched expansion restricts γI_{eff} while the hose requirement restricts γ/I_{eff}. In addition, we limit the beam energy to $\gamma \lesssim 21$, in order to avoid nuclear activation of the target. Together, these three limits circumscribe a range of values allowed for γ and I_{eff}.

The range of allowed parameters is illustrated in Fig. 5 which shows three curves representing the limits imposed by beam expansion (solid curve), resistive hose (dashed curve), and avoidance of nuclear activation (dot-dashed curve). In this parameter regime, $I_{eff} \simeq I_b$, so that the results are plotted in terms of I_b versus beam energy. In all of the cases shown in Fig. 5, it is assumed that the beam is injected in equilibrium with a radius of $a_o = 0.1$ cm, that the expansion on target is restricted to $g_a \leq \sqrt{2}$, and that propagation is in full-density air. In Fig. 5a, the propagation distance is $z_t = 10$ cm, the allowed hose growth is $g_h \leq 30$, and there is no straw. In that case the (shaded) area circumscribed by the three curves is large, indicating considerable flexibility in the choice of beam current and energy. In Fig. 5b, the propagation distance is increased to $z_t = 20$ cm, which reduces the allowed parameter range. At $z_t = 30$ cm (Fig. 5c), the beam parameters are tightly constrained to $I_b \simeq 1$ kA and $\mathcal{E} \simeq 10$ MeV.

A wide parameter range for propagation to $z_t = 30$ cm can be recovered by propagating the beam inside a conducting straw of radius $a_w = 3$ mm. As shown in Fig. 6a, the beam energy can then be as low as $\mathcal{E} \simeq 6$ MeV, with the current increased to $I_b \simeq 1.6$ ka. With the use of a straw to guide the beam, a reasonable choice of parameters is available even if the criterion for acceptable hose growth is reduced to a conservative $g_h \leq 10$. The allowed parameter range is substantially larger still if the straw is filled with helium, or with air at reduced density. The case of He at atmospheric density (equivalent to air at 40 torr) is shown in Fig. 6b, which indicates that the beam energy can be as low as 1 MeV. In addition, in all cases the required propagation

parameters can be relaxed if the beam radius is allowed to be several mm or more on target. (In fact, the on-target radius may have to be larger than 1 mm, in order to avoid shocking the material, for typical beam pulse lengths of several tens of ns; moreover, radii ~ 2 mm do not appreciably compromise weld strength, but do reduce the need for tight joint tolerances.) Overall, we conclude that narrow beams of high energy density can be readily delivered to targets located 30 cm or more from the accelerator, without need of vacuum pumping.

B. Particle-Simulation Results

The analytical estimates given for beam expansion and hose instability in the previous sections make a number of simplifying assumptions which are marginal in some cases. To relax these assumptions and obtain a more detailed treatment, we use the three-dimensional, nonlinear particle simulation code SARLAC, which incorporates gas scattering, ohmic and collisional energy loss, and a set of rate equations for computing the plasma conductivity.[41] The beam is taken to be ultrarelativistic ($\gamma >> 1$) and paraxial ($v_\perp << v_z$), so the retarded time $\tau \equiv t - z/c$ is a constant of the motion for the beam particles. The beam propagates in a gas-filled conducting straw with a radius a_w that can be much larger than the beam radius a_b. The independent variables are r, θ, τ, and z, where θ is the azimuthal angle about the axis of the straw. With these assumptions, Maxwell's equations and the conductivity rate equations contain no derivatives in z, whereas the equations of motion for the beam particles contain no derivatives in τ. The code allows for variations in the beam radius, current, and energy within the pulse.

The beam was injected with current I_b rising rapidly to 1 kA, energy $\gamma = 21$, radius $a_0 = 0.1$ cm (but slightly larger at early τ), and pulse length shortened to $\tau_p = 2$ ns to conserve computer time. The beam was loaded with a Bennett radial distribution, and a transverse temperature matched to pinch current $I_{eff} = 0.85$ kA. At $z = 0$, initial sinusoidal hose displacements $x_i(\tau)$ and $y_i(\tau)$ were applied in both the x and y directions. The amplitude of these initial perturbations was 10^{-3} cm, and the frequency of x_i was set to $\omega/2\pi = 1$ GHz, while the frequency of y_i was set to 5 GHz. (In the linear regime, the perturbations of the beam in the x-z plane and in the y-z plane evolve independently.) The use of a shortened τ_p and only two discrete hose perturbation frequencies leads to a slight underestimate of the maximum possible hose growth.

In the first set of simulations, the radius of the straw was set to $a_w = 5$ cm, which is large enough so that wall effects should be negligible. The beam half-current radius $a_b(\tau)$ is plotted at two z locations in Fig. 7a. As is evident, the beam slowly expands and its head gradually erodes as it propagates. Hose growth for the slice at $\tau = 0.75$ ns is shown by the solid curve in Fig. 7b. Maximum hose growth occurred at somewhat later τ, with a peak growth of $g_h = 25$ at $z = 30$ cm. This agrees well with the analytic prediction of $g_h < 35$ given earlier (for the most unstable perturbation frequency and unlimited pulse length).

In the second set of simulations, the same beam [with its density $n_b(r)$ cut off at the straw radius a_w] was propagated inside a conducting straw of radius $a_w = 3$ mm. As shown by the dashed curve in Fig. 7b, the straw reduced the peak hose growth to $g_h = 5$ at $z = 30$ cm. Again, this agrees well with the analytic prediction of $g_h < 8$. The loss of beam current due to scrape-off on the straw is shown in Fig. 7c to be only five percent.

To test for wall steering, the preceding simulation was repeated except that the beam was injected misaimed at an angle $dx/dz = 10$ mrad. As shown in Fig. 7d, the beam slice at $\tau = 0.75$ ns oscillated about a peak displacement of 0.35 mm with a wavelength $\lambda \approx 28$ cm. This displacement and wavelength agree well with analytic prediction. The figure also shows that hose growth is unaffected by the misaiming.

V. OTHER ISSUES

A. Gas Heating

In gas, electron beams deposit energy directly into excited states and the plasma electron population, and this energy is shared later with the translational, vibrational, and other degrees of freedom of the gas. The heating and equilibration of the gas produces a reduced-density channel, with an eventually elevated plasma conductivity σ. For a single isolated HEEB pulse (which may be suitable for some applications), these effects have no significant impact on propagation, because the pulse length is too short for appreciable gas expansion to occur, and because increases in σ in the beam tail have virtually no effect on pinching or overall hose growth.

However, in a repetitive mode, late beam pulses encounter the hot air channel formed by their predecessors, and the effect of this channel on beam propagation depends sensitively on the channel temperature. At channel temperatures below 3000 K (and pulse repetition rates below 10 kHz), the plasma recombines between pulses, and the heated channel expands. The beam pulses then enter a rarefied but non-conducting channel that retards Nordsieck expansion of the beam. In addition, the radial density gradient in the channel alters the beam-generated conductivity, and this leads to a weak channel-guiding force on the beam.[42,43]

At temperatures above ~ 3500 K, the effect of the channel changes abruptly. At these temperatures, the channel remains ionized and highly conducting between pulses. A fresh beam pulse entering the preionized channel induces a plasma return current that fully neutralizes the beam current, and this current magnetically ejects the beam from the channel. The transition from channel guiding to channel ejection has been observed[43] to occur at a temperature ~ 3500 K. Very hot channels thus deflect subsequent beam pulses away from the target. At the high current densities required for HEEB welding, channel temperatures can reach 3500 K after a few pulses.

One way to avoid channel overheating is to blow the channel away. An unlimited number of beam pulses can then propagate, since each pulse encounters essentially virgin gas. An air flow speed of a few m/s across the channel is sufficient for pulse rates less than a few kHz. In open air, natural convection may provide sufficient cooling. If the beam is propagated in a straw, it may be necessary to blow gas through the straw, or out through perforations.

B. Beam Deflection

With the low-energy beams presently used for welding, beam deflection by stray magnetic fields is a significant problem.[4,6,8] The high-energy beams discussed in this paper are so stiff that they are virtually impervious to naturally occurring magnetic fields localized on the workpiece surface. However, magnetic fields induced by the beam, and external fields that act coherently over the entire beam path, may still be of significance. A convenient measure of these effects is the value of the perpendicular magnetic field B_o which, acting over the entire propagation length, is sufficient to deflect the beam by an amount equal to its radius a_b:

$$B_o = \frac{2a_b I_A}{z_t^2 c} . \qquad (40)$$

For our canonical HEEB parameters, $B_o = 8$ G. The earth's magnetic field (0.3 G) is therefore unimportant, and deflection from power lines is usually unimportant provided the cables lie a meter or more away from the beam.

A more significant concern is the image currents and charges induced by the beam in nearby conductors. Consider a beam propagating in open air parallel to a ground plane. The net current (the sum of I_b and the induced plasma current) induces an equal but opposite image current in the ground plane, and this current produces a magnetic field of strength $B_g = I_n/xc$ on the beam located a distance x away. This magnetic field would tend to deflect the beam away from the ground plane. The field B_g exceeds B_o when $x \leq (z_t^2/2a_b)(I_n/I_A)$. For our canonical welding beam parameters, this occurs when $x \leq 12.6$ cm. Thus this simple calculation would appear to indicate that magnetic deflection could be a significant problem.

Fortunately, there are a number of effects that can greatly reduce the strength of the interaction between a beam and a nearby ground plane. A brief catalog of these effects would include the following: (i) Image *charges* are also induced in the conductor, and the resulting electrostatic forces are opposite in sign to the magnetic image forces. If the beam is highly relativistic, these forces are very nearly equal and opposite to the magnetic forces. (ii) However, the plasma channel surrounding the beam can shield, to differing degrees, both the magnetic and electrostatic image forces. Usually, the electrostatic forces are shielded much more effectively

than the magnetic forces. (iii) Under some circumstances, there are significant time delays for the transmission of fields from the beam to the conductor and back. (iv) The deflecting force on the beam rises from zero with τ, due to variations in $I_b(\tau)$, $\sigma(\tau)$, etc. Thus the deflecting forces tend to send different parts of the beam off at different trajectories. (v) However, there are also strong coupling forces (mediated by the plasma channel) that hold the beam together, and force the body of the beam to follow the trajectory established by the head. In a recent paper,[44] we sorted through these issues in considerable detail, and concluded that ground plane deflection is essentially absent when two conditions are met: the beam must be highly relativistic, $\gamma > 5$; and it must have sufficient current to ionize the gas rapidly, in the sense that

$$s_i I_b > a_b/x \quad , \tag{41}$$

where $s_i = (e/2m\nu W_i c^2)(d\epsilon/dz)$ is a beam ionization coefficient. Under these conditions, the beam body follows the trajectory determined by the head. At the head of the beam, there is not enough plasma to neutralize the beam fields, and thus the head is not deflected significantly because the electric and magnetic image forces cancel (to order γ^{-2}). In air, $s_i \approx 0.04\ kA^{-1}$, which leads to the prediction that ground-plane deflection becomes unimportant at distances $x > 3$ cm for our canonical welding beam. If it is necessary to propagate the beam closer than 3 cm to a ground plane, the beam should be propagated inside a conducting straw, to shield it from outside induced fields.

An additional deflection mechanism arises in welding from asymmetrical currents induced in the melt pool.[8] If these currents were confined to one side of the joint, the beam could be deflected by its radius in a penetration distance as short as $\lambda_\beta/4$, which is 3 cm for the nominal parameters given earlier. In practice, however, the distance is much longer because the currents are not unilaterally distributed. Consequently, beam deflection within the melt pool should not be a problem, even for welds as deep as 10 cm.

C. Matching

In the preceding calculations, we assumed that the beam enters in pinched equilibrium with $T_\perp = T_B$, a Bennett radial profile, and a radius suitable for the application. If the beam is injected out of equilibrium, the beam radius and profile will oscillate. However, as described in the hose

analysis, these oscillations will damp as the beam electrons get out of phase with one another in the anharmonic pinch potential. Phase-mixing thus causes the beam to approach a quiescent steady state after roughly one betatron wavelength of propagation.[45] Phase-mix damping increases, however, the beam emittance.[24]

A beam injected with a matched temperature $T_\perp = T_B$ but a non-equilibrium radial profile will experience only modest emittance growth,[45] provided the plasma return current is much smaller than I_b, as is true for the parameters considered here, and provided the injected profile falls off smoothly with r. Thus it is not particularly important for our applications to launch a beam whose radial profile is well-matched.

On the other hand, to prevent the beam from over-expanding at the target, the temperature at injection should kept at or below T_B. If the beam is injected cold, $T_\perp < T_B$, it will collapse under the action of the pinch force, but the transverse energy acquired during collapse will push the electrons back out, so that the equilibrated radius[24] is smaller than the injected radius only by a factor $\sim \sqrt{2}$. That is, the beam acquires enough emittance during equilibration to prevent significant, permanent collapse. A related point is that the injected radius a_o should be no larger than that desired at the target, since emittance growth prevents the beam from contracting much below a_o. At the same time, a_o should not be much smaller than needed, since this increases hose growth. In general, therefore, the beam should be injected with a_o slightly less than needed at the target, and with $T_\perp \leq T_B$.

VI. CONCLUSION

The advent of high-power, high-energy, repetitive electron beams offers new possibilities for electron beam welding and materials processing. In this report, we have focused on the potential of these beams to propagate tightly pinched (with radius ~ 1 mm) through a few tens of cm in ambient air, without need of external guide fields. This capability would eliminate the need for vacuum pumping at the target and for magnetic focusing at the accelerator. Furthermore, the use of high-energy electrons offers the potential for improved deep welding, due to the long range of the electrons in the target material and the constancy of the beam radius in the "keyhole" made within the target.

After reviewing the physics of self-pinched propagation in gas, our major conclusion is that propagation is an important but not overriding issue for most applications. That is, the limitations imposed by propagation are significant but do not severely restrict the utilization of the technology. The three most important limitations are: gas scattering, which limits the minimum beam power; hose instability, which limits the maximum beam current; and the need to avoid nuclear activation, which limits the maximum beam energy. The restrictions on beam current and energy become stressing if the beam is required to remain small (a_b ~ 0.1 cm) while propagating over a significant standoff to the target. The nominal parameters needed to propagate through 30 cm of full density air are 1 kA and 10 MeV; these values are sensitive to the desired beam range and can be reduced if the standoff distance is reduced. The margin of safety can be increased by propagating the beam inside a conducting "straw" which reduces hose growth, eliminates concerns regarding beam deflection from stray or beam-induced fields, and can reduce gas scattering if the straw is differentially pumped or filled with a gas like helium. In the regime of interest, the beam pulse length is not limited by propagation considerations.

In short, the advantages of high-power electron beams for welding and materials processing can apparently be realized, provided pulsed high-power beam sources become available with cost and reliability comparable to that of the low-power dc generators being used commercially today. These advantages include: the ability to propagate to the target in ambient air without need of vacuum pumping or magnetic focusing; the ability to deposit energy deep within the target; the ability to heat the target rapidly to minimize thermal losses and to excite shocks if desired; and

the ability to fine-tune the time history of the deposition. Finally, it is quite feasible to test the propagation predictions made here using scaled experiments which can be performed with presently available, high-power pulsed beam sources.

ACKNOWLEDGEMENTS

We thank Eugene Nolting for initiating this work and continuing to discuss it with us, and we thank A. C. "Chip" Smith and William Fawley for sharing their related work with us. In addition, we are grateful to Glenn Joyce and Steven Slinker for use of and consultations on the particle code SARLAC, and we acknowledge Jonathan Fernsler for assisting with the figures. This work was supported by the Office of Naval Research and by the Advanced Research Projects Agency, under ARPA Order 7781, as monitored by the Naval Surface Warfare Center.

REFERENCES

1. B. W. Schumacher and D. E. Powers, Industrial and Production Engineering **13**, 47 (1989).
2. B. W. Schumacher, Welding J. **52**, 312 (May 1973).
3. E. Gajdusek, Welding J. **59**, 17 (July 1980).
4. A. Sanderson and K. R. Nightingale, Welding J. **69**, 45 (April 1990).
5. R. C. Smith and B. W. Schumacher, Nucl. Instr. Meth. **118**, 73 (1974).
6. T. W. Eager, Welding J. **65**, 19 (July 1986).
7. J. H. Fink, Welding J. **54**, Res. Suppl. 137 (May 1975).
8. S. A. David and T. Debroy, Science **257**, 497 (1992).
9. J. F. Lowry, J. H. Fink, and B. W. Schumacher, J. Appl. Phys. **47**, 95 (1976).
10. A. C. Smith and E. E. Nolting, "An Overview of High Energy Electron Beam Science," in *Proceedings of the Premier Conference and Workshop on High Energy Electron Beam Welding and Materials Processing*, 1992 (American Welding Society, Miami, 1993).
11. See *Proceedings of the Premier Conference and Workshop on High Energy Electron Beam Welding and Materials Processing*, 1992 (American Welding Society, Miami, 1993).
12. B. N. Turman, M. G. Mazarakis, and E. L. Neau, "Fundamentals of High Energy Electron Beam Generation," ibid.
13. R. A. Meger, J. K. Burton, J. R. Greig, D. P. Murphy, M. C. Myers, M. C. Nash, R. E. Pechacek, M. Raleigh, and D. P. Taggart, in *Proceedings of the Sixth IEEE Pulsed Power Conference* (Institute of Electrical and Electronics Engineers, New York, 1987), p. 502.
14. C. A. Kapetanakos, L. K. Ken, T. Smith, J. Golden, K. Smith, S. J. Marsh, D. Dialetis, J. Mathew, P. Loschialpo, and J. H. Chang, Phys. Rev. Lett. **64**, 2374 (1990).
15. C. A. Frost, S. L. Shope, M. G. Mazarakis, J. W. Poukey, G. T. Leifeste, and C. E. Crist, Bull. Am. Phys. Soc. **35**, 931 (1990).
16. K. W. Struve, G. J. Caporaso, Y. P. Chong, J. C. Clark, T. J. Fessenden, E. J. Lauer, D. S. Prono, J. T. Weir, and F. W. Chambers, "Status of Beam Transport with the ETA and ATA Accelerators," NTIS Document No. DE84013205, 1984. Copies may be ordered from the National Technical Information Service, Springfield, VA 22161.

17. D. S. Prono, et al., in *Proceedings of the 1989 IEEE Particle Accelerator Conference* (Institute of Electrical and Electronics Engineers, Piscataway, NJ, 1989), p. 1441.
18. D. S. Prono, IEEE Trans. Nucl. Sci. **NS-32**, 3144 (1985).
19. Y. Hoshi and K. Mizusawa, Nucl. Instr. Meth. **B56-57**, 1236 (1991).
20. M. R. Cleland, C. C. Thompson, H. Kato, M. Odera, R. F. Morrissey, C. M. Herring, M. T. O'Neil, T. R. Wilcott, J. Masefield, J. M. Hansen, M. C. Saylor, and D. P. Sloan, Nucl. Instr. Meth. **B56-57**, 1242 (1991).
21. T. Sadat, Nucl. Instr. Meth. **B56-57**, 1226 (1991).
22. See, for example, J. D. Jackson, *Classical Electrodynamics* (Wiley, New York, 1967).
23. J. Benford and J. Swegle, *High Power Microwaves* (Artech House, Boston, 1992).
24. R. F. Fernsler, R. F. Hubbard, and S. P. Slinker, Phys. Fluids. **B4**, 4153 (1992).
25. R. F. Hubbard, S. P. Slinker, R. F. Fernsler, G. Joyce, and M. Lampe, J. Appl. Phy. **73**, 4181 (1992).
26. R. F. Hubbard, J. A. Antoniades, R. F. Fernsler, M. Lampe, R. A. Meger, D. P. Murphy, R. Pechacek, T. A. Peyser, and S. P. Slinker, "Beam Conditioning and Propagation Experiments on SuperIBEX," in *Intense Microwaves and Particle Beams III*, Proc. SPIE **1629**, (International Society for Optical Engineering, Bellington, WA, 1992), p. 392.
27. E. P. Lee, Phys. Fluids **19**, 60 (1976).
28. A similar but incomplete result was given as Eq. (1) in Ref. 7. The present result should give better agreement with experiment.
29. T. P. Hughes and B. B. Godfrey, Phys. Fluids **27**, 1531 (1984).
30. W. M. Sharp and M. Lampe, Phys. Fluids **23**, 2383 (1980).
31. R. L. Platzman, International J. Appl. Radiation and Isotopes **10**, 116 (1961).
32. R. F. Fernsler, R. F. Hubbard, B. Hui, G. Joyce, M. Lampe, and Y. Y. Lau, Phys. Fluids **29**, 3056 (1986).
33. E. J. Lauer, R. J. Briggs, T. J. Fessenden, R. E. Hester, and E. P. Lee, Phys. Fluids **21**, 1344 (1978).
34. M. Lampe, R. F. Fernsler, and R. F. Hubbard, "Fundamentals of HEEB Propagation," in *Proceedings of the Premier Conference and Workshop on High Energy Electron Beam Welding and Materials Processing*, 1992 (American Welding Society, Miami, 1993).

35. E. P. Lee, Phys. Fluids **21**, 1327 (1978).

36. M. Lampe, W. M. Sharp, R. F. Hubbard, E. P. Lee, and R. J. Briggs, Phys. Fluids **27**, 2921 (1984).

37. R. F. Fernsler, S. P. Slinker, R. F. Hubbard, and M. Lampe, in *Proceedings of the 9th International Conference on High-Power Particle Beams*, NTIS Document No. PB92-206168, p. 1276, 1992. Copies may be ordered from the National Technical Information Service, Springfield, VA 22161.

38. W. M. Sharp, M. Lampe, and H. S. Uhm, Phys. Fluids **25**, 1456 (1982).

39. H. S. Uhm and M. Lampe, Phys. Fluids **23**, 1574 (1980).

40. G. Joyce and M. Lampe, Phys. Fluids **26**, 3377 (1983).

41. G. Joyce, R. Hubbard, M. Lampe, and S. Slinker, J. Comput. Phys. **81**, 193 (1989).

42. R. F. Fernsler, S. P. Slinker, and R. F. Hubbard, Phys. Fluids **B3**, 2696 (1991).

43. D. P. Murphy, R. E. Pechacek, D. P. Taggart, R. F. Fernsler, R. F. Hubbard, S. P. Slinker, and R. A. Meger, Phys. Fluids **B4**, 3407 (1992).

44. R. F. Fernsler and M. Lampe, Phys. Fluids **B3**, 3177 (1991).

45. R. F. Hubbard, M. Lampe, S. P. Slinker, and G. Joyce, Phys. Fluids **31**, 2349 (1988).

APPENDIX: RESISTIVE HOSE ISSUES

In this appendix, we refine the analysis given for the resistive hose instability in the presence of a conducting straw. In particular, we show that the straw reduces the dipole decay time τ_d according to Eq. (33), and we include the effects of orbit phase-mixing.

To compute the dipole decay time, we drop electrostatic effects and axial derivatives from Ampere's law, leaving[35]

$$\nabla_{\perp}^2 A_z = - \frac{4\pi}{c} \left[j_b - \frac{\sigma}{c} \frac{\partial A_z}{\partial \tau} \right] , \qquad (A1)$$

where A_z is the axial vector potential. The neglect of electrostatics is justified provided the plasma conductivity is high, $4\pi\sigma_o a_b/c >> 1$, while the neglect of axial derivatives is justified provided the beam is energetic, $\gamma >> 1$, and paraxial, $\lambda_\beta >> a_b$. To simplify the analysis further, we assume that the plasma conductivity σ follows the beam and is distributed with the same radial profile. The straw imposes the boundary condition that $A_z = 0$ at $r = a_w$.

For small displacements x_b from the axis of the straw, the beam current density can be expanded in the (r,θ) plane as

$$j_b(r,\theta,\tau) = j_b(r,0,\tau) - x_b(\tau) \cos\theta \frac{\partial}{\partial r} j_b(r,0,\tau) + \ldots \qquad (A2)$$

The plasma conductivity σ can be expanded similarly, while the potential A_z can be expanded as

$$A_z(r,\theta,\tau) = A_w(r,\theta,\tau) + A_o(r,\tau) - x_n(\tau) \cos\theta \frac{\partial A_o}{\partial r} + \ldots \qquad (A3)$$

Here x_n is the displacement of the net-current centroid, and A_w is the contribution to the vector potential due to the image current $-I_n$ located at a_w^2/x_n from the axis of the straw. For $x_n << a_w$ and $r < a_w$,

$$A_w(r,\theta,\tau) = - \frac{2I_n}{c(a_w^2/x_n)} r \cos\theta . \qquad (A4)$$

Substituting expressions (A2)-(A4) into Eq. (A1) yields separate monopole and dipole equations. The monopole equation for A_o is given by

$$\frac{1}{r}\frac{\partial}{\partial r} r \frac{\partial}{\partial r} A_o = -\frac{4\pi}{c}\left[j_b - \frac{\sigma}{c}\frac{\partial A_o}{\partial \tau}\right] = -\frac{4\pi}{c} j_n \ , \qquad (A5)$$

where j_n is identified as the net-current density. Solutions to this equation show that A_o relaxes on the L/R time discussed in Sec. II-E.

The corresponding dipole equation is

$$\frac{\partial}{\partial r}\frac{1}{r}\frac{\partial}{\partial r} rA_1 = \frac{4\pi}{c}\left[x_b \frac{\partial j_n}{\partial r} + \frac{\sigma}{c}\frac{\partial A_1}{\partial \tau}\right] \ , \qquad (A6)$$

where A_1 is the dipole potential given by

$$A_1 = -x_n \frac{\partial A_o}{\partial r} - x_n \frac{2I_n}{a_w c}\frac{r}{a_w}$$

$$= x_n \frac{2}{rc}\left[i_n(r) - \left(\frac{r}{a_w}\right)^2 I_n\right] \ . \qquad (A7)$$

Here we have used the fact that the monopole magnetic field is given from Eq. (A5) by $B_\theta = -\partial A_o/\partial r = 2i_n(r)/rc$, where

$$i_n(r) = \int_0^r dr' \ 2\pi r' j_n \qquad (A8)$$

is the net current enclosed within radius r and $I_n = i_n(a_w)$. Inserting Eq. (A7) into Eq. (A6) produces, after some manipulation,

$$\left[1 - \frac{I_n}{i_n(r)}\left(\frac{r}{a_w}\right)^2\right]\left[\frac{-2\sigma i_n}{rc^2 \partial j_n/\partial r}\right]\frac{\partial x_n}{\partial \tau} = x_b - x_n \ , \qquad (A9)$$

where we have taken I_n to be constant in time.

If σ and j_n have the same Bennett profile of radius a_b, the term

$$\frac{-2\sigma i_n}{rc^2 \partial j_n/\partial r} = \pi\sigma_o a_b^2/2c^2 \equiv \tau_{do} \qquad \text{(A10)}$$

is independent of r. This is a unique property of Bennett profiles, and it justifies treating the dipole field as a simple displacement of the monopole field, plus a contribution from the wall current.

Equation (A9) shows that a straw reduces the relaxation time of the dipole field from τ_{do} to

$$\tau_d = \left[1 - \frac{I_n}{i_n(r)}\left(\frac{r}{a_w}\right)^2\right] \tau_{do}$$

$$= \left(\frac{a_w^2 - r^2}{a_w^2 + a_b^2}\right) \tau_{do} \qquad \text{(A11)}$$

for Bennett profiles. The dependence on r is weak for most of the beam if $a_w \geq 3\, a_b$, and it can be "removed" by averaging over the beam to define an effective dipole decay time given for Bennett profiles by

$$\langle\tau_d\rangle = \tau_{do} \frac{1}{I_b} \int_0^{a_w} dr \frac{\partial i_b}{\partial r} \left[1 - \frac{I_n}{i_n(r)} \left(\frac{r}{a_w}\right)^2\right]$$

$$= \tau_{do}\left[1 - (a_b/a_w)^2 \ln(1+a_w^2/a_b^2)\right] . \qquad \text{(A12)}$$

For flat-topped profiles, averaging is not needed, and $\tau_d/\tau_{do} = (1-r_b^2/a_w^2)$, where r_b is the edge radius given by Eq. (30); this reduction is evident in the analysis of Uhm and Lampe.[39] Not surprisingly, the reduction is roughly the same for Bennett profiles when expressed in terms of r_b.

Let us now add orbit phase mixing. Phase mixing occurs when the local pinch force, proportional to $i_n(r)/r$, does not increase linearly with r. The betatron oscillation frequency of the beam electrons then varies with r, attaining its maximum value $k_{\beta o}$ on the beam axis. To model this variation without following the three-dimensional trajectories of individual electrons, Lee[35]

represented each slice of the beam by an ensemble of components, each of which has a Bennett radial profile and is allowed to undergo transverse displacements without internal distortion. However, each component is assigned a beam electron mass which is weighted by a variable $\eta \leq 1$, so that a component oscillates at a betatron frequency $\sqrt{\eta}\, k_{\beta o}$. The distribution of masses $f(\eta)$ was chosen to be the simplest form that satisfies certain conservation properties. Overall, the spread-mass model gives good results, partly because the hose growth rate is insensitive to details in $f(\eta)$.

Each mass component separately satisfies Eq. (31), which can be written as

$$\frac{\partial^2}{\partial z^2} x_{b\eta} = \eta k_{\beta o}^2 \left(x_n - x_{b\eta}\right) - \left(r_b/a_w\right)^2 k_s^2 x_n$$

$$= \eta k_{\beta o}^2 \left(x_n - x_{b\eta}\right) - \left(a_b/a_w\right)^2 k_{\beta o}^2 x_n \,, \qquad \text{(A13)}$$

where $r_b k_s = a_b k_{\beta o}$ for Bennett profiles. This equation applies for all η between 0 and 1. Observe that we did *not* apply phase-mixing to the wall force because that force, unlike the self-pinch force, is independent of position and is therefore the same for all particles in a given slice.

To derive a dispersion relationship, we impose solutions of the form $x \sim e^{-ikz - i\omega\tau}$ on Eqs. (A9) and (A13). That reduces Eq. (A13) to

$$x_{b\eta} = \frac{\eta k_{\beta o}^2 - \left(a_b/a_w\right)^2 k_{\beta o}^2}{\eta k_{\beta o}^2 - k^2} x_n \,, \qquad \text{(A14)}$$

and Eq. (A9) to

$$x_b \equiv \int_0^1 d\eta\, f(\eta)\, x_{b\eta} = \left(1 - i\omega\tau_d\right) x_n \,, \qquad \text{(A15)}$$

where τ_d is the effective dipole decay time given by Eq. (A12). We then integrate Eq. (A14) over $f(\eta)$ and combine it with Eq. (A15) to obtain

$$-i\omega\tau_d = \left[1 - \left(a_b/a_w\right)^2 \chi^{-1}\right] G(\chi) \,, \qquad \text{(A16)}$$

where $\chi = k^2/k_{\beta o}^2$ and the spread-mass function G is defined by

$$G(\chi) = \int_0^1 d\eta \; f(\eta) \; \frac{\chi}{\eta - \chi} \; . \qquad (A17)$$

Equation (A16) is the spread-mass dispersion relationship in the presence of wall forces.

The functions $f(\eta)$ and $G(\chi)$ depend on the radial structure of $i_n(r)$. A straw can alter $i_n(r)$ by restricting the maximum orbit radius of the beam electrons; this reduces the spread in orbit frequencies and forces $f(\eta)$ to zero at small η. However, the net effect on phase mixing and $G(\chi)$ is not severe, provided the orbit frequencies vary by two or more inside the straw. This is easily met for Bennett profiles if $a_w \geq 3\, a_b$. We shall therefore impose this restriction and use $G(\chi)$ as calculated by Lee in the absence of wall forces. For unbounded Bennett profiles,[35]

$$G(\chi) = 6\chi \left[\frac{1}{2} - \chi + \chi(1-\chi) \; \ln\left[\frac{1-\chi}{\chi} \right] \right] \; . \qquad (A18)$$

If growth in z is more important than growth in τ, we can take ω to be real. The real part of the right-hand side of Eq. (A16) then equals zero, yielding

$$(a_b/a_w)^2 = \frac{\mathrm{Re}\{G(\chi)\}}{\mathrm{Re}\{G(\chi)/\chi\}} \equiv F(k_r, k_i) \; . \qquad (A19)$$

The peak growth rate k_i^{max} occurs where $\partial F/\partial k_r = 0$. This allows us to compute k_i^{max} as a function of a_b/a_w. In Fig. 4, we plot $k_i^{max}/k_{\beta o}$ as a function of a_b/a_w using the Bennett spread-mass function given by Eq. (A18). Recall that this function improperly includes contributions from outside the straw, so that the analysis becomes suspect at $a_w < 3a_b$. For comparison, we also show the flexible-rod result (dashed curve). The good agreement between the two curves indicates that phase-mixing reduces k_i^{max} only moderately.

To complete the analysis, we compute the peak growth rate ω_i^{max} in τ for real k. Recall that ω_i^{max} becomes important if $z_t/\lambda_\beta >> \tau_p/\tau_d$. For real k, Eq. (A16) yields

$$\omega_i \tau_d = \left[1 - (a_b/a_w)^2 \chi^{-1} \right] \mathrm{Re}\{G(\chi)\} \; , \qquad (A20)$$

where $\chi = (k_r/k_{\beta o})^2$ is real. For a given a_b/a_w, the peak growth is easily determined and is plotted in Fig. 8, using Eq. (A12) to account for the reduction in τ_d due to the straw. The growth rate is

everywhere finite because phase-mixing spreads the resonance at $k = k_s$. A comparison of Figs. 4 and 8 shows that a straw lowers k_i^{max} more than ω_i^{max}, for $a_w \geq 3a_b$.

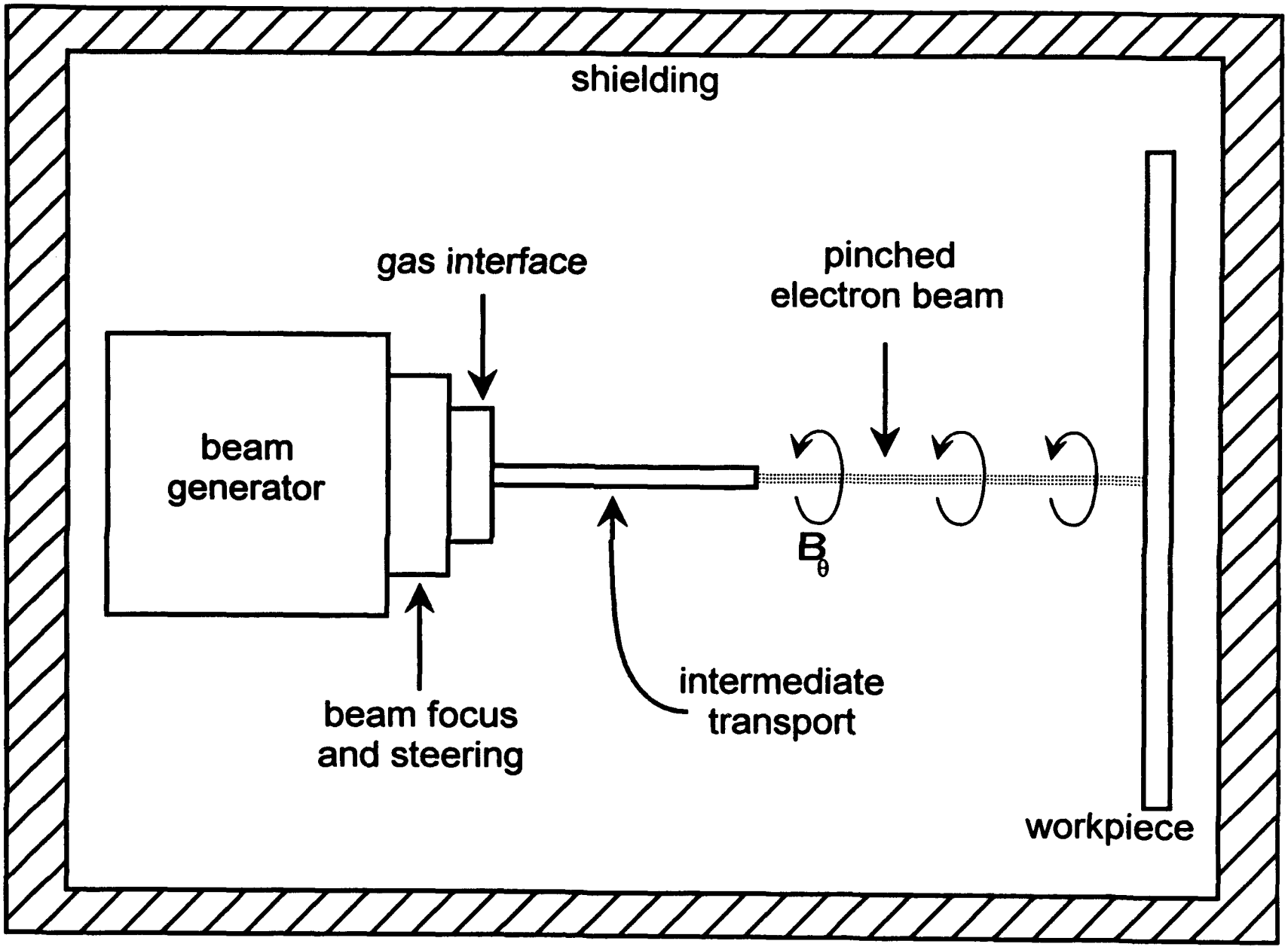

Fig. 1 – Generic welding or materials processing system consisting of: a pulsed beam generator; a focusing and steering section (if required); an intermediate transport section (e.g., a straw); a free transport zone; various vacuum/ gas interfaces; and x-ray shielding surrounding the entire unit.

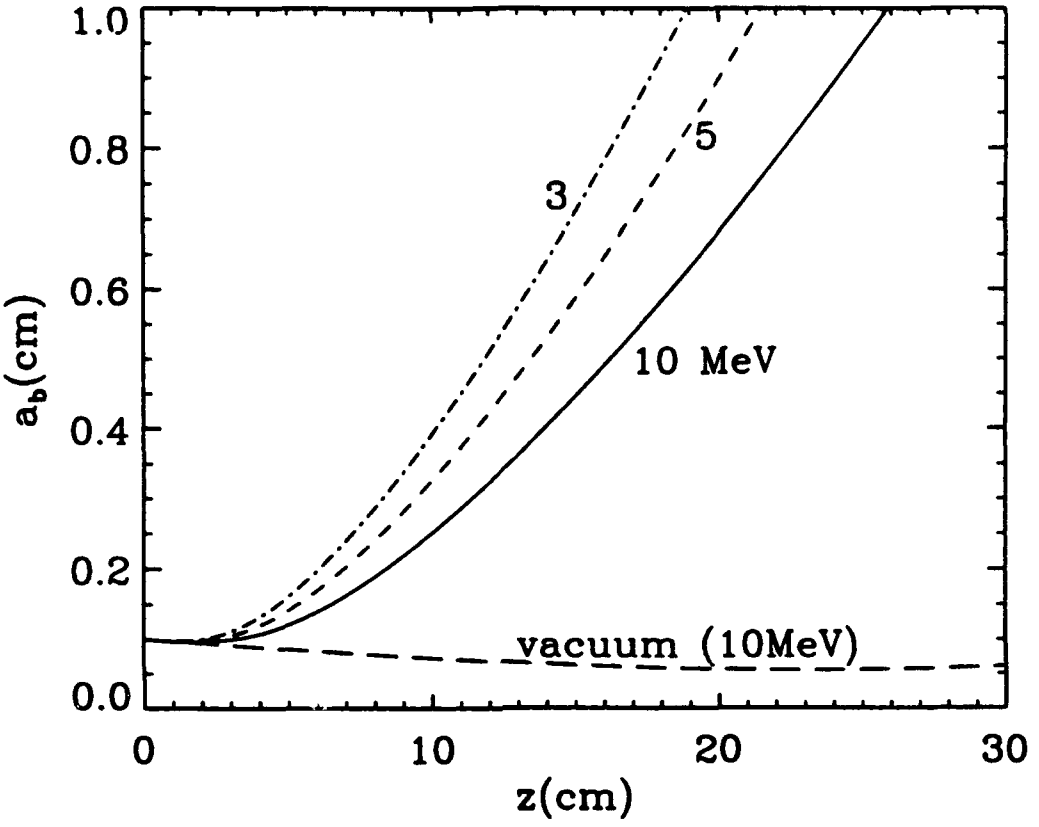

Fig. 2 – Free expansion in air and vacuum for $\theta_f = 0.003$, $\theta_i = 0.002$, and beam energies of 3, 5, and 10 MeV

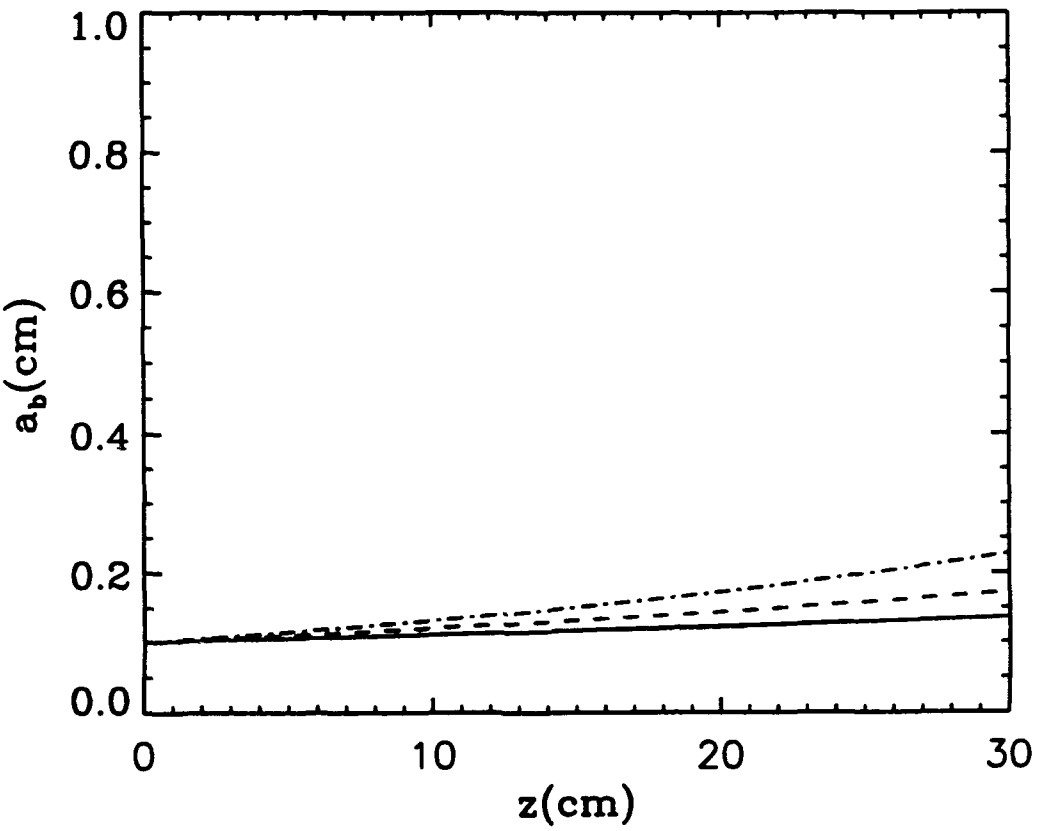

Fig. 3 – Self-pinched expansion in air for I_{eff} = 1 kA at 3 MeV (dot-dashed), 5 MeV (dashed), and 10 MeV (solid)

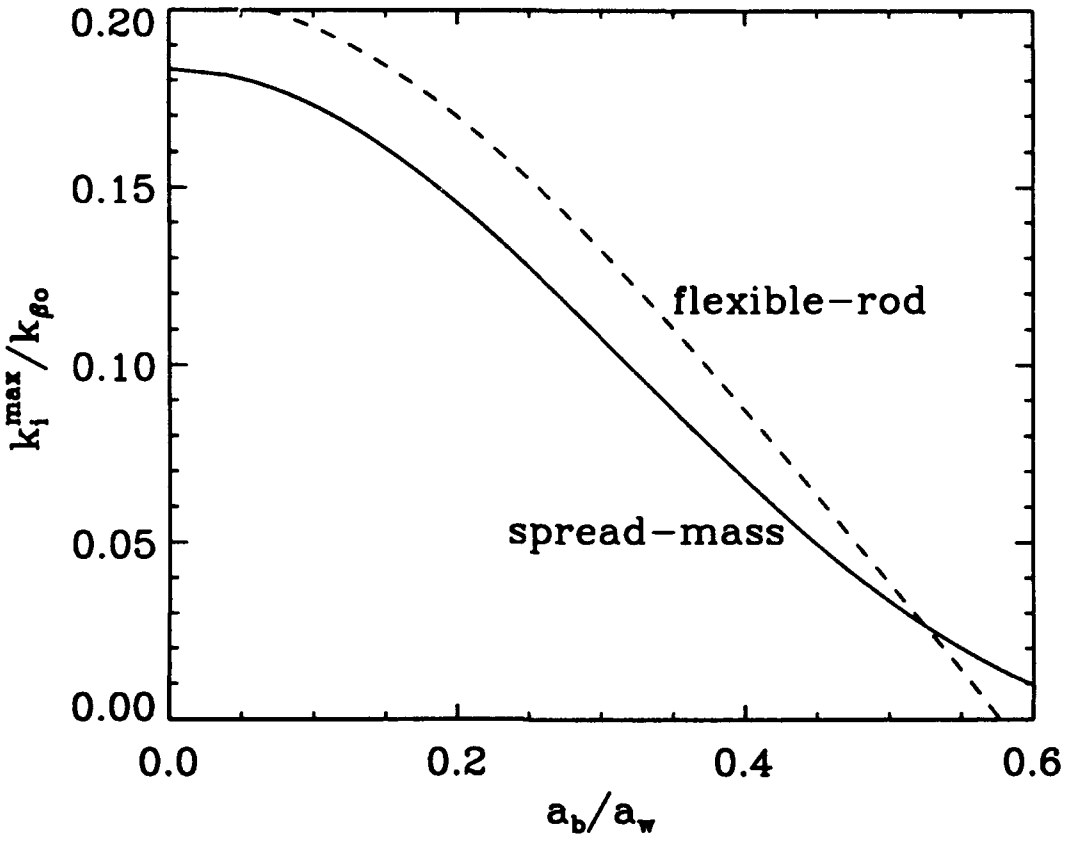

Fig. 4 – Peak hose growth rate in z as a function of beam/straw radius

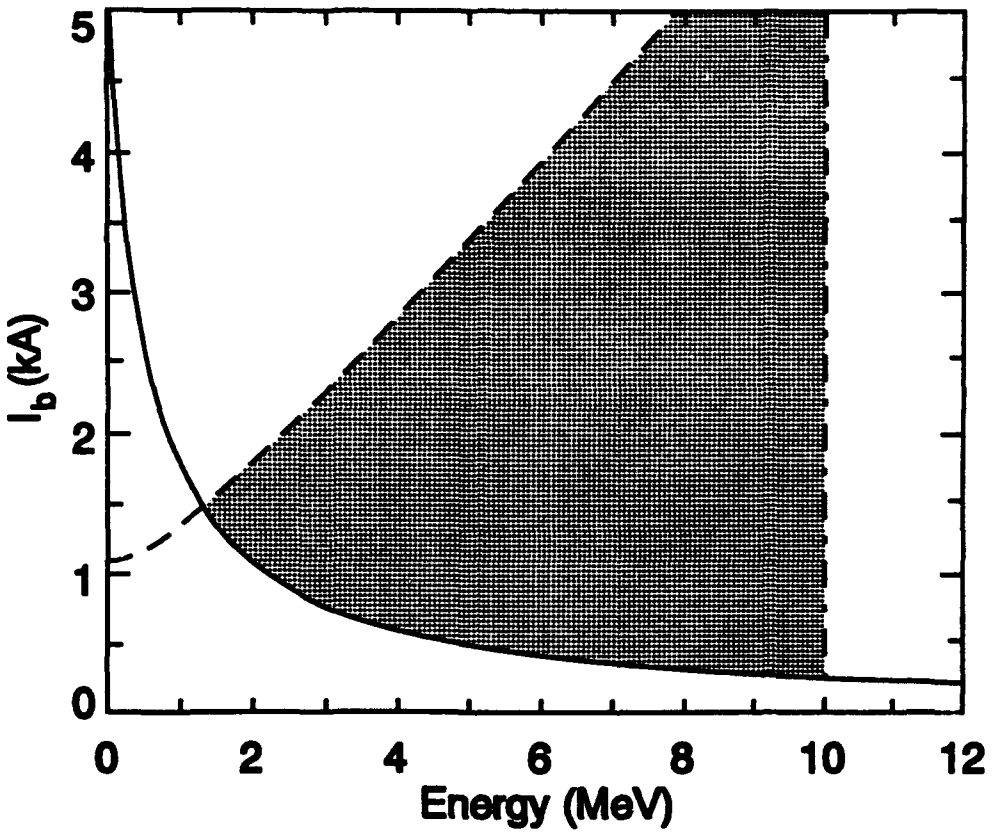

Fig. 5a – Allowed beam current and energy (shaded region) for $z_t = 10$ cm, $a_o = 0.1$ cm, $a_w = \infty$, $g_a \leq \sqrt{2}$, and $g_h \leq 30$

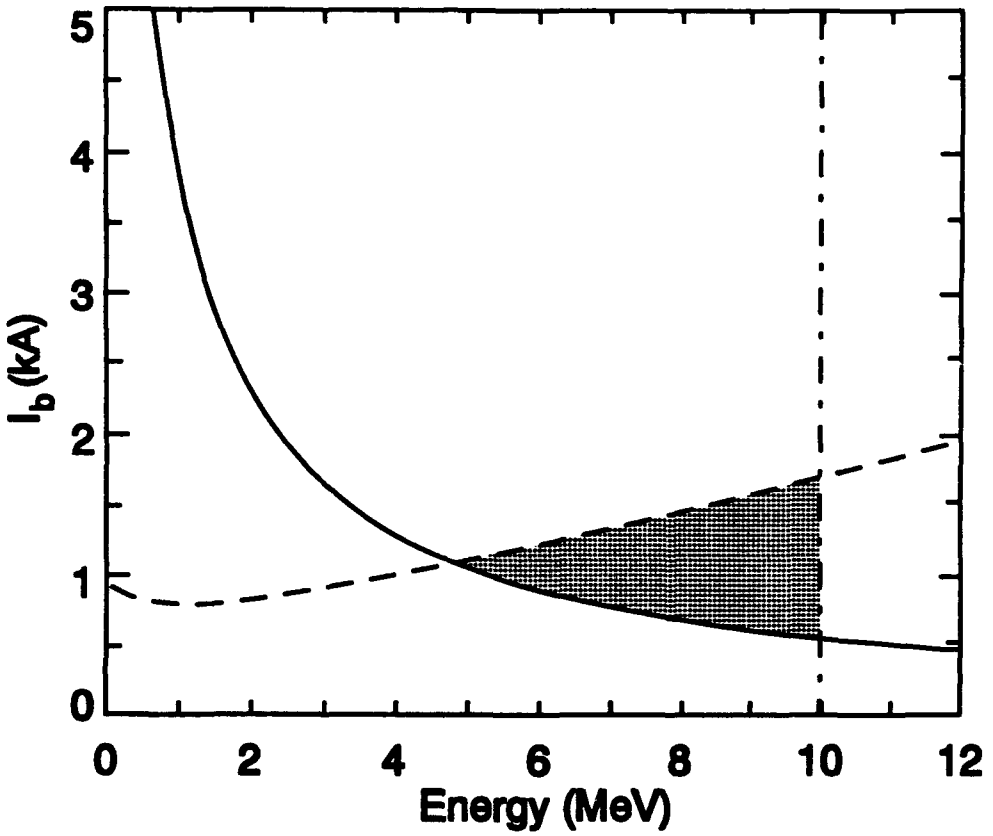

Fig. 5b – Allowed parameters for z_t = 20 cm

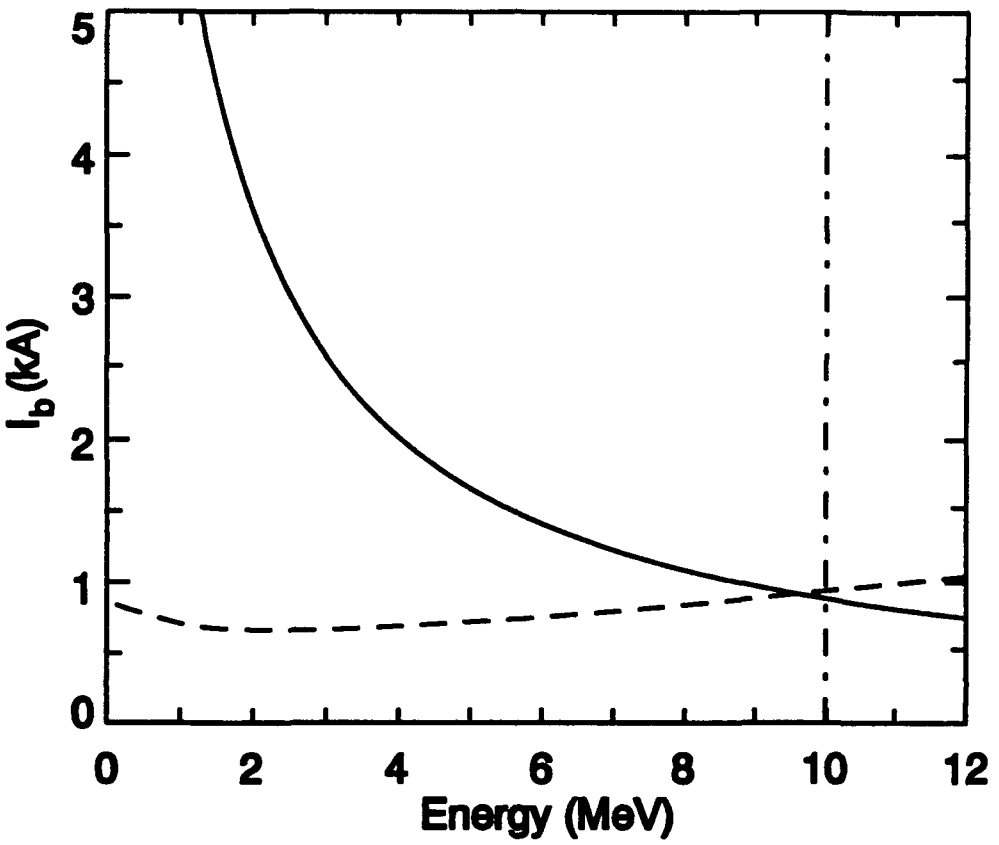

Fig. 5c – Allowed parameters for z_t = 30 cm

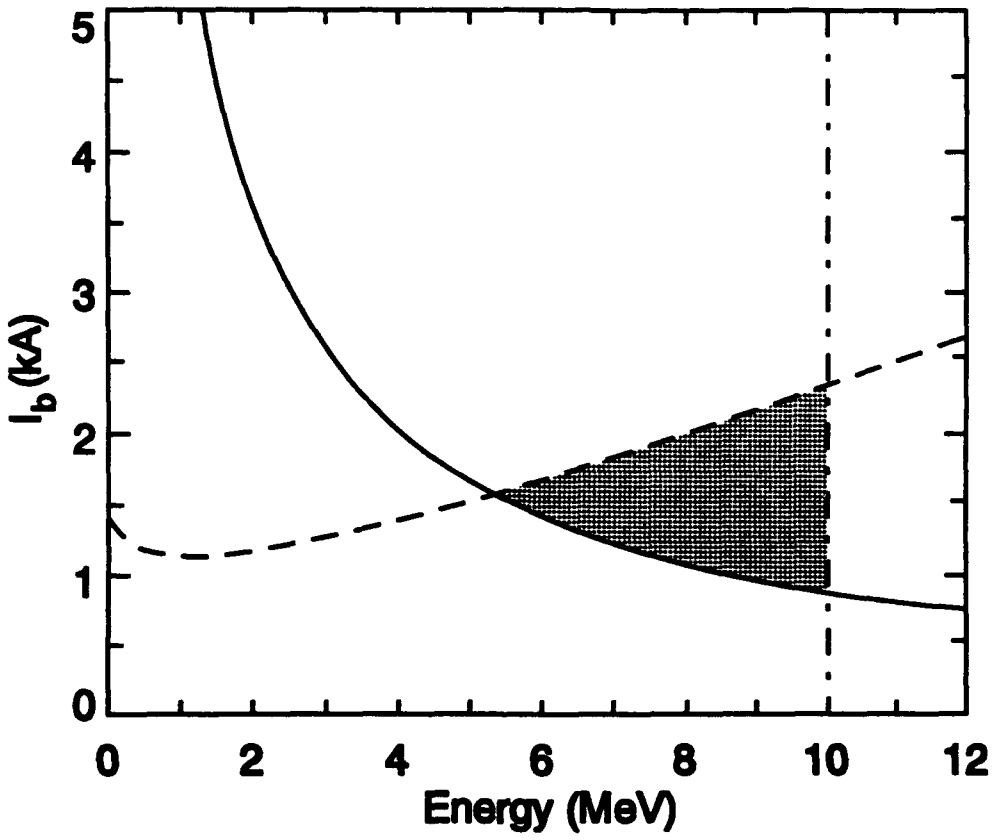

Fig. 6a – Allowed parameters at $z_t = 30$ cm using a straw of radius $a_w = 3a_o$

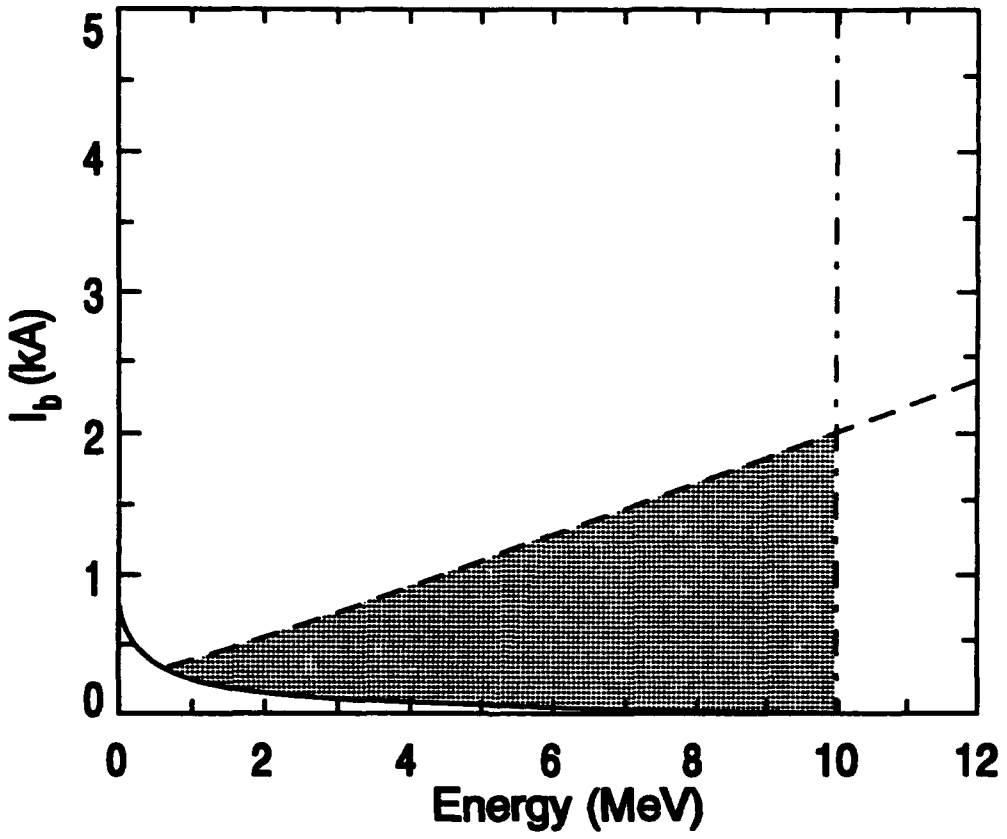

Fig. 6b – Allowed parameters using a straw filled with 1 atm of He

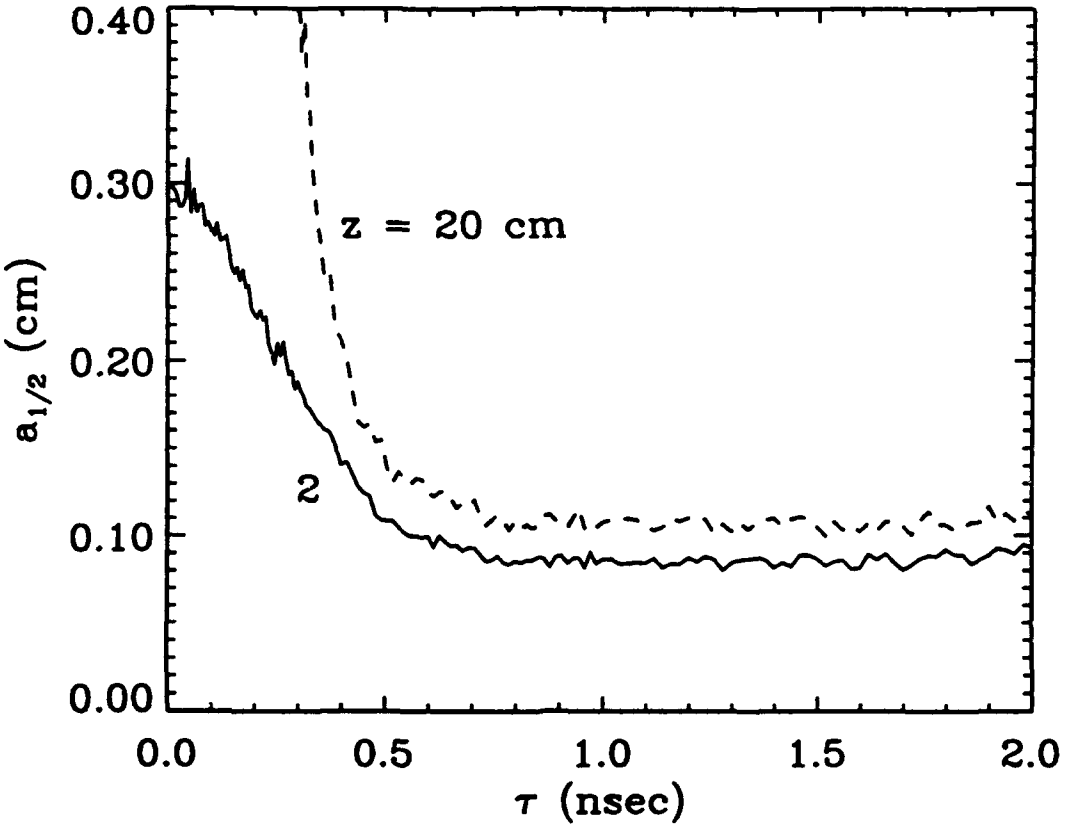

Fig. 7a – Half-current radius from SARLAC at two z locations

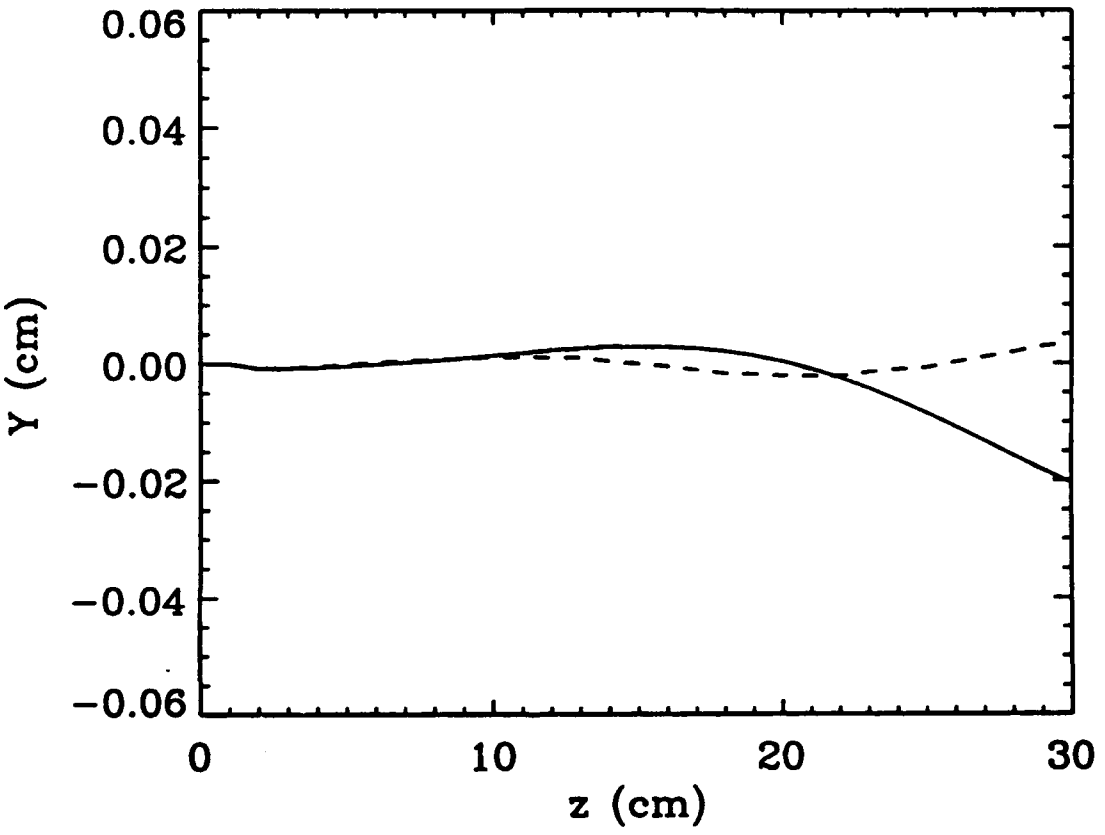

Fig. 7b – Beam centroid as a function of z with (solid curve) and without (dashed curve) a straw

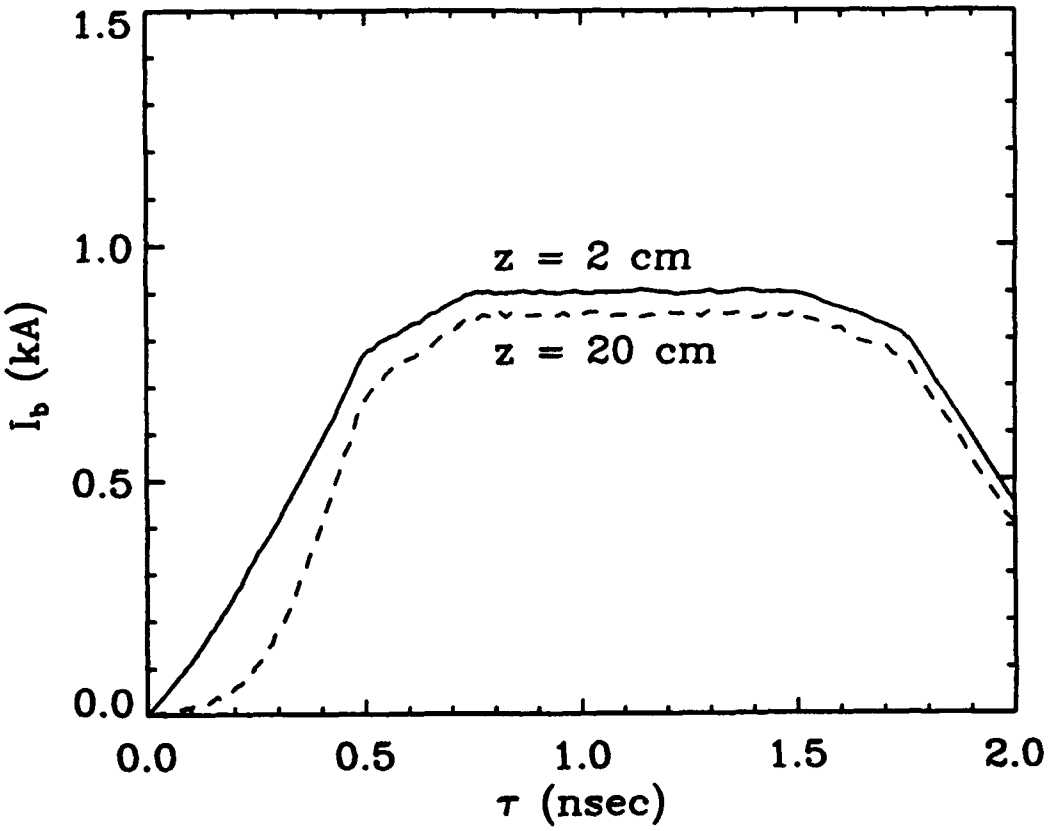

Fig. 7c – Loss of beam current inside a straw

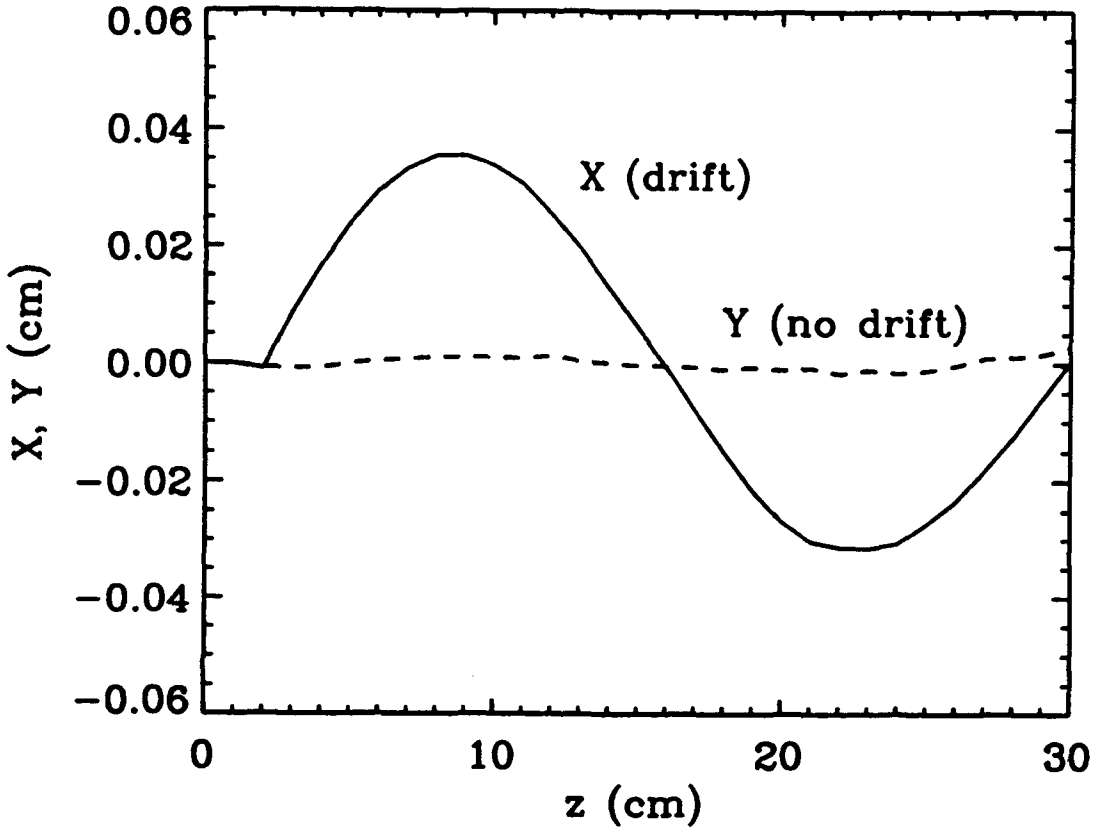

Fig. 7d – Centroid of a beam injected at an angle of dx/dz = 10 mrad from the axis of the straw

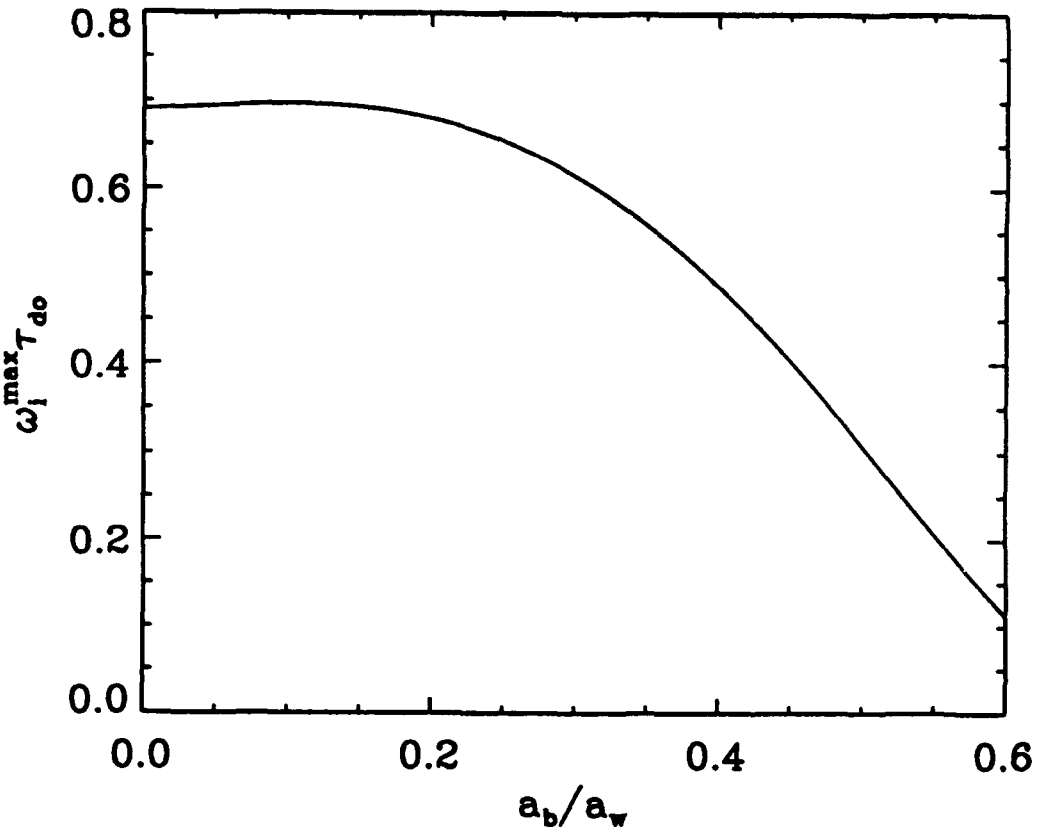

Fig. 8 – Peak hose growth rate in τ as a function of beam/straw radius